

¹ **Copyright**
² **by**
³ **Ryan Patrick Hannigan**
⁴ **2023**

5 The Dissertation Committee for Ryan Patrick Hannigan certifies that
6 this is the approved version of the following dissertation:

7 Stranger Things at the LHC

Committee:

Christina Markert, Supervisor

Peter Onyisi

Aaron Zimmerman

Chandrajit Bajaj

8

9

Stranger Things at the LHC

10

by

11

Ryan Patrick Hannigan, Ph.D.

12

Dissertation

13

Presented to the Faculty of the Graduate School of

14

The University of Texas at Austin

15

in Partial Fulfillment

16

of the Requirements

17

for the degree of

18

Doctor of Philosophy

19

The University of Texas at Austin

20

May, 2023

To Jaynee.

22

Stranger Things at the LHC

23

Publication No. _____

24

Ryan Patrick Hannigan, Ph.D.

25

The University of Texas at Austin, 2023

26

Supervisor: Christina Markert

Abstract

28 Quantum chromodynamics (QCD) is the branch of fundamental particle physics that
 29 studies the strong interaction, which is responsible for binding quarks and gluons into
 30 the familiar protons and neutrons that compose almost all ordinary matter. One of
 31 the most exciting predictions of this theory is the existence of a new state of matter,
 32 known as the quark-gluon plasma (QGP). At extreme temperatures and densities,
 33 protons and neutrons dissolve into their constituent quarks and gluons, forming a
 34 soup-like plasma of deconfined partons. This QGP is thought to have existed in the
 35 early universe, thus studying its formation and properties can help answer questions
 36 about the evolution of the universe and the nature of the strong force. However,
 37 recreating the extreme conditions of the early universe can be achieved by smashing
 38 together heavy nuclei at *very* high energies. This can only be done at the world's
 39 most powerful particle accelerators¹.

40 Unfortunately, QGP produced in these collisions only lasts for around 10^{-23} sec-
 41 onds, making it impossible to study the plasma directly. Instead, there are a few key
 42 experimental observables that are associated with the characteristics of this plasma
 43 which can be studied. One such signature of QGP formation is known as strangeness
 44 enhancement, where the production of strange quarks within the QGP is enhanced
 45 relative to the standard up and down quarks that compose protons and neutrons.
 46 Previously believed to be unique to heavy-ion collisions, recent measurements have
 47 indicated that this enhancement is also present in high multiplicity proton-proton (pp)
 48 and proton-lead (p-Pb) systems as well. These measurements hint at the formation
 49 of a QGP in these smaller collision systems, calling into question the prediction that
 50 the formation of this plasma is only possible in heavy-ion collisions. While statistical
 51 and phenomenological models are capable of describing this enhancement in these
 52 smaller collision systems, the microscopic origins of strangeness enhancement are not
 53 well understood.

54 Jets, which are streams of hadrons produced by an initial hard scattering of the
 55 partons within the colliding nuclei, can be used to illuminate the underlying pro-
 56 cesses that produce these strange particles. By measuring the angular correlation

¹Making the QGP the most expensive soup on the menu.

57 between a high-momentum trigger hadron (as a proxy for a jet axis) and a lower
58 momentum strange hadron, it is possible to differentiate the strangeness-producing
59 mechanisms between hard (jet-like) and soft (underlying event) processes. This an-
60 gular correlation technique can be used to study the production of strangeness as a
61 function of multiplicity in these regimes, giving insight into the origins of the observed
62 enhancement.

63 This thesis presents the first results utilizing azimuthal angular correlations to
64 measure the production of Λ baryons—which are composed of an up, a down, and
65 a strange quark (uds)—in p-Pb collisions at $\sqrt{s_{NN}} = 5.02$ TeV using the ALICE
66 detector at the LHC. The correlation measurements are used to extract the Λ jet-like
67 and underlying event yields, as well as obtain the widths of the jets to provide more
68 context for the observed jet production. These results are studied as a function of
69 the Λ momentum and collision multiplicity, which are used to quantify the enhance-
70 ment of strange quark production in these different kinematic regimes. Comparisons
71 with theoretical predictions are also made to provide a framework for interpreting the
72 results of this thesis. Moreover, these yield measurements are compared with pub-
73 lished measurements of the $\phi(1020)$ meson ($s\bar{s}$), which utilized similar techniques, to
74 investigate the differences between open ($|S| > 1$) and hidden ($|S| = 0$) strangeness
75 production. These strange measurements provide new insight into the production
76 of strangeness in smaller collision systems, thus further constraining the microscopic
77 origins of strangeness enhancement.

Chapter One: Introduction

79 The initial section of this chapter will mostly serve as a historical overview of the
80 field of particle physics, leading to the development of the **Standard Model**: the
81 theory that describes all of the fundamental¹ particles and the way in which they
82 interact with each other. An emphasis will be made on the discovery of quarks and
83 gluons, as the research presented in this thesis is centered around these particles.
84 The second section will more thoroughly introduce the Standard Model and its three
85 distinct sectors, with the goal to provide a high-level mathematical overview of the
86 theory.

87 The third section of this chapter will delve into the details of Quantum Chromo-
88 Dynamics (QCD), which is the component of the Standard Model that describes the
89 interactions between **quarks** and **gluons**, the constituent particles of the more famil-
90 iar protons and neutrons. As many theoretical calculations are difficult to perform
91 in QCD, the use of computationally-intensive numerical techniques is often required
92 to make precise predictions. One such prediction is a phase transition from nuclear
93 matter at everyday energies—in which the quarks and gluons are confined within
94 protons and neutrons—into a novel state of matter at extreme temperatures or den-
95 sities, known as the **Quark-Gluon Plasma** (QGP). Section 1.4 will detail the QGP
96 and many of its interesting properties predicted by QCD, with an emphasis on the
97 production of strange quarks within the plasma.

98 The final two sections of this chapter will discuss how high-energy particle col-
99 lisions can be used to study the QGP, using both expensive particle accelerators
100 (Section 1.5) and simulation techniques (Section 1.6).

¹As of the year 2023, but reading this chapter will hopefully illustrate why this may be subject to change in the (likely very distant) future.

101 1.1 What is fundamental?

102 The answer to the question

103 What are the fundamental building blocks of our universe?

104 has changed drastically over the course of human history. The idea that all matter
105 is composed of smaller, uncuttable pieces has been around since 5th century BCE
106 when Greek philosophers Democritus and Leucippus first introduced the concept of
107 an atom [1]. While this idea was mostly motivated by philosophical reasoning, it was
108 later adopted by the English scientist John Dalton in the 19th century to explain the
109 results of his chemical experiments, where he found that chemical elements always
110 combined with each other by discrete units of mass [2]. As scientists discovered more
111 and more of these elements, the number of “fundamental” building blocks grew as
112 well. By the late 1800s, over 70 unique chemical elements had been discovered, though
113 they would often be grouped together due to similar chemical properties using what
114 chemist Dimitri Mendeleev dubbed the *periodic table of elements* [3]. An example of
115 the periodic table from the time of Mendeleev can be seen in Figure 1.1. While this
116 grouping was useful for chemists, it also served as a hint to physicists that perhaps
117 these elements were not actually fundamental, but rather composed of even smaller
118 pieces.

		Ti = 50	Zr = 90	? = 180
		V = 51	Nb = 94	Ta = 182
		Cr = 52	Mo = 96	W = 186
		Mn = 55	Rh = 104,4	Pt = 197,4
		Fe = 56	Ru = 104,4	Ir = 198
		Ni = Co = 59	Pd = 106,6	Os = 199
H = 1		Cu = 63,4	Ag = 108	Hg = 200
	Be = 9,4	Zn = 65,2	Cd = 112	
	B = 11	Al = 27,4	? = 68	Uu = 197?
	C = 12	Si = 28	? = 70	Sn = 118
	N = 14	P = 31	As = 75	Sb = 122
	O = 16	S = 32	Se = 79,4	Te = 128?
	F = 19	Cl = 35,5	Br = 80	J = 127
Li = 7	Na = 23	K = 39	Rb = 85,4	Cs = 133
		Ca = 40	Sr = 87,6	Tl = 204
		? = 45	Ce = 92	Pb = 207
		?Er = 56	La = 94	
		?Yt = 60	Di = 95	
		?In = 75,6	Th = 118?	

Figure 1.1: Dimitri Mendeleev’s periodic table of elements from the late 1800s, taken from [4]. The elements are grouped by similar chemical properties, and the gaps in the table are where Mendeleev predicted that new elements would be discovered.

119 Scientists' understanding of the building blocks of matter changed again around
120 the turn of the 20th century, with physicists J.J. Thomson, Ernest Rutherford, and
121 James Chadwick determining that the supposedly indivisible atom was composed
122 of even smaller subatomic particles, eventually named electrons, protons, and neu-
123 trons [5]–[7]. Thus the number of fundamental blocks of matter had decreased sub-
124 stantially from nearly 100 to just three. However, this number would need to be
125 updated again only months later, as the fundamental anti-particle of the electron—
126 known as the positron—was discovered in 1932 by Carl Anderson [8]. In the next two
127 decades, the number of known fundamental particles would skyrocket. In 1947, the
128 muon was discovered [9], followed by the discovery of a laundry list of particles [10]–
129 [12] that participate in the same interaction that holds the positively charged protons
130 together in the nucleus of an atom—the so-called **strong nuclear force**. These “fun-
131 damental” particles were collectively called **hadrons**, which were further separated
132 into lighter and heavier categories, dubbed **mesons** and **baryons**, respectively [13].
133 By the late 1960s, the number of known hadrons had grown to well over 100 [14],
134 even more than the number of “fundamental” chemical elements that were known to
135 exist in the 1800s.

136 In the same way that Mendeleev tried to group the elements by their similar
137 chemical properties, physicists attempted to group the hadrons together based on
138 their known subatomic properties. The first successful attempt at such a grouping
139 was the **Eightfold Way**, which was independently proposed by Murray Gell-Mann
140 and Yuval Ne’eman in 1961 [15], [16]. This grouping was found by examining the
141 following properties of the hadrons:

- 142 1. **Isotopic spin:** a quantum number introduced by Werner Heisenberg in 1932
143 to try to explain the apparent symmetries between the proton and neutron
144 with respect to the strong nuclear force [17] (i.e. although the proton and
145 neutron have different electric charges, the strong interaction does not seem to
146 distinguish between the two)
- 147 2. **Strangeness:** another quantum number introduced by Gell-Mann and Nishi-
148 jima in 1953 to explain why some hadrons decayed much more slowly than
149 expected, and such particles appeared to be created in pairs [18]. In other
150 words, the strong interaction responsible for the creation of these particles ap-
151 peared to conserve this quantum number, but the weak interaction responsible

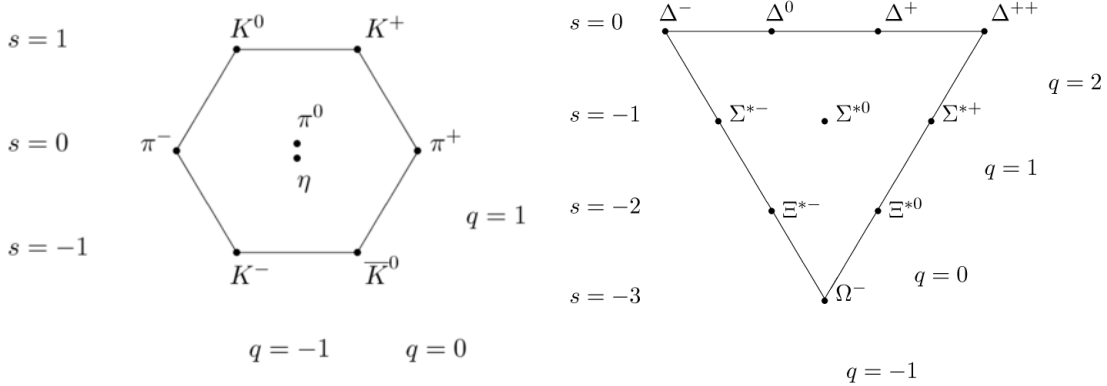


Figure 1.2: The “Eightfold Way” diagrams of the $J = 1/2$ mesons (left) and $J = 3/2$ baryons (right) plotted against strangeness and electric charge. Understanding the underlying symmetry group that gives rise to such patterns³ ultimately led to the development of the quark model. While the original patterns were found using isotopic spin and hypercharge, it is trivial to convert between the two using the Gell-Mann-Nishijima formula [19], [20].

152 for the slower decay of these particles did not. Strangeness² will be discussed
 153 in more detail in Section 1.3.2.5.

154 Plotting the baryons and mesons in a two-dimensional space based on these two
 155 properties revealed striking patterns, as shown in Figure 1.2. Similar to Mendeleev,
 156 GellMann also left a blank space⁴ where he believed a new particle—the Ω^- —would
 157 be discovered. The patterns in these diagrams hinted at an underlying symmetry
 158 governing the strong nuclear force, and ultimately led to the invention of the very
 159 first quark model by Gell-Mann and Zweig in 1964 [21]. This model proposed that
 160 all of the hadrons were actually composed of even smaller particles, which Gell-Mann
 161 dubbed “quarks”. The quark model was able to explain the patterns seen in Figure 1.2
 162 by introducing three different types of fermionic quarks—up, down and strange—along
 163 with their corresponding anti-quarks. Baryons would then be composed of three such

²The “strangeness” being referred to in this section was introduced a few years before the very first quark model, but it now has the modern interpretation which is directly related to the number of strange and anti-strange quarks within a hadron.

³Namely $SU(3)$, but this is a history lesson. Also the path from $SU(3)$ to patterns of this type is long and arduous, involving a thorough understanding of representation theory.

⁴The original paper on the Eightfold Way does not contain any of these diagrams, but there are discussions about the properties of particles that should exist if the theory were correct, but had not been observed [15].

164 quarks, whereas mesons would be composed of quark and anti-quark pairs. If the
165 quark model were correct, the number of fundamental building blocks of matter would
166 again decrease from over 100 to just 14: electrons, muons, electron neutrinos, muon
167 neutrinos, up quarks, down quarks, strange quarks, and all of their corresponding
168 anti-particles.

169 Initially, many physicists believed that the quarks from this model were just a
170 mathematical abstraction [22]. This possibility did not stop Sheldon Glashow and
171 James Bjorken from extending the quark model less than a year after its inception by
172 introducing a fourth quark: the charm [23]. This new quark was primarily introduced
173 to equalize the number of leptons (four at the time: electron, muon, and their re-
174 spective neutrinos) with the number of quarks. The theory was mostly aesthetic [24]
175 in that the charm quark was not explicitly required by any known mechanisms. It
176 was only after the Glashow-Iliopoulos-Maiani (GIM) mechanism was introduced in
177 1970 [25] that the existence of the charm quark became necessary. This mechanism
178 helped explain why neutral kaons decayed into two muons at a much lower rate than
179 expected, but it required the existence of a quark with the same charge as the up
180 quark but with a much larger mass.

181 The notion that protons and neutrons were fundamental particles was also being
182 challenged on the experimental side. The deep inelastic scattering experiments at the
183 Stanford Linear Accelerator Center (SLAC) performed by Kendall, Friedman, and
184 Taylor in 1968 [26]–[28] revealed unexpected⁵ behavior when probing the structure
185 of the proton: it appeared to be composed of point-like particles. These experiments
186 were performed by firing electrons at stationary protons and measuring the energy
187 distributions of the scattered electrons at different scattering angles. An example
188 of such a distribution for electrons with initial energies of 10 GeV scattered at 6
189 degrees can be seen in Figure 1.3. The large spike on the left side of the distribution
190 corresponds to the elastic scattering of the electron off the proton, which was well
191 understood at the time [29]. The “bumps” observed at lower values of the scattered
192 electron energy were also well understood [30], and they correspond to the “shallow”
193 inelastic scattering of the electron off the proton, where the proton gets excited into a
194 so-called *resonance* state (like the Δ baryon). However, the “background” underneath
195 the bumps and the apparent continuum of events at even lower values of the scattered

⁵Depending on who you asked at the time, both the three and four quark models were not universally accepted.

196 electron energy corresponded to a host of unknown particles being produced. This
 197 host of particles appeared to grow with increasing scattering angle and decreasing
 198 scattered electron energy, which ultimately led to the conclusion that the proton was
 199 composed of point-like particles that were being “knocked out” of the proton by the
 200 incoming electron [26], [31].

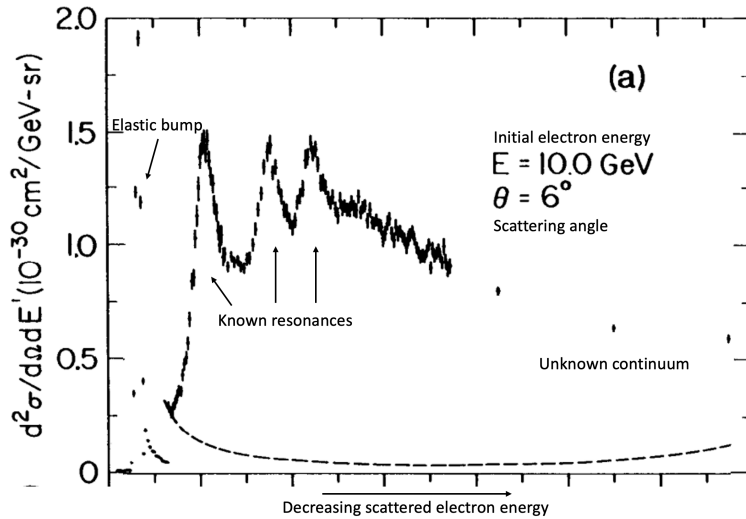


Figure 1.3: The energy distribution of electrons scattered off of protons at an initial electron energy of 10 GeV and a scattering angle of 6 degrees. The large spike on the left side of the distribution corresponds to the elastic scattering of the electron off the proton, and the “bumps” correspond to the inelastic scattering of the electron off the proton. The “background” underneath the bumps and the apparent continuum of events at even lower values of the scattered electron energy correspond to a mess of unknown particles being produced. The behavior of this continuum with respect to the scattering angle and the scattered electron energy ultimately led to the conclusion that the proton was not fundamental.

201 While many physicists were perfectly happy to interpret these point-like parti-
 202 cles as the very same quarks from the aforementioned quark model(s), they received
 203 the much more noncommittal name **partons** after Richard Feynman’s parton model
 204 of hadrons [32]. The association of these partons with quarks was not universally
 205 accepted⁶ until the discovery of the J/ψ meson in 1974 [33]. In the meantime, the
 206 theoretical description of the strong nuclear force was closing in on its final form.

⁶No acceptance of any model is a step function, but the discovery of J/ψ seems to be a turning point in literature.

207 The formulation of Quantum ChromoDynamics (QCD) in the early 1970s by Gell-
208 Mann, Fritzsch, and Leutwyler [34] resolved many of the issues that were present in
209 the initial quark models⁷. QCD introduced the concept of color charge, which all of
210 the quarks would carry. The mediating bosons of the strong interaction—known as
211 **gluons**—were also introduced, carrying color charge as well.

212 While QCD gave a solid mathematical description of the strong interaction, it
213 wasn’t until the discovery of **asymptotic freedom** [35], [36] by Gross, Wilczek, and
214 Politzer in 1973 that the theory became experimentally testable. Asymptotic freedom
215 refers to the property that the strong interaction becomes weaker at higher energies,
216 allowing for QCD calculations to be performed using perturbative techniques. This
217 discovery allowed theorists to use QCD to make predictions of the results of very
218 high energy particle collision experiments. The first QCD prediction to be experimen-
219 tally verified came from the Positron-Electron Tandem Ring Accelerator (PETRA)
220 in 1979 [37], which experimentally confirmed the existence of gluons [38]. With ex-
221 perimental verification of QCD, it became clear that the association of partons with
222 quarks was indeed incorrect: they are both quarks *and* gluons.

223 In addition to the theory of QCD, the theory of electroweak interactions was
224 also being developed during the 1960s by Glashow, Weinberg, and Salam [39], [40].
225 With this new theory came the prediction of four⁸ new bosons: the Higgs boson, the
226 charged W^\pm bosons, and the neutral Z^0 boson. With the combined theories of the
227 electroweak and strong interaction, the **Standard Model** of particle physics—which
228 describes the now 61⁹ fundamental particles and how they interact—was complete.

229 1.2 The Standard Model

230 The Standard Model of particle physics is a **quantum field theory** (QFT) that
231 describes the interactions between all¹⁰ of the fundamental particles. QFTs describe
232 the dynamics of a quantum system in terms of fields, which are functions of space and

⁷For example, the wavefunction of the Δ^{++} baryon under the first quark model was not anti-symmetric, which is a requirement for fermions.

⁸The Higgs mechanism (which predicts the existence of the Higgs boson) came before electroweak unification [41], but it was a requirement for the theory.

⁹There are many ways to count fundamental particles, but this particular number is obtained by: 6 leptons ($\times 2$ for anti-leptons), 6 quarks ($\times 3$ for each color, $\times 2$ for anti-quarks), 1 gluon ($\times 8$ for color), 1 photon, the W and Z bosons, and the Higgs boson.

¹⁰Ignoring potential gravitons [42] or dark matter candidates [43]

233 time. The fields are the fundamental objects of QFT, and their excitations correspond
234 to the particles that are observed in nature. The Standard Model fields can be broken
235 down into three sectors, which will be discussed in the following sections.

236 **1.2.1 The gauge sector**

237 The gauge sector of the Standard Model corresponds to the spin-one bosons that
238 mediate the strong and electroweak interactions. In a general sense, this sector corre-
239 sponds to the mediating particles for three of the four fundamental forces: the strong
240 nuclear force, the weak nuclear force, and the electromagnetic force. The fourth
241 fundamental force—gravity—is not included in the Standard Model, as it is not yet
242 understood from a quantum perspective [44].

243 The symmetry group of the gauge sector is given by

$$\text{SU}(3)_c \times [\text{SU}(2)_L \times \text{U}(1)_Y]. \quad (1.1)$$

244 $\text{SU}(3)_c$ is the symmetry group of the strong interaction, which is described by the QFT
245 known as Quantum ChromoDynamics (QCD). The subscript c stands for “color”,
246 indicating that the gauge fields in QCD (gluons) only couple to colored objects. QCD
247 will be discussed in more detail in Section 1.3. The symmetry group of the electroweak
248 interaction is $\text{SU}(2)_L \times \text{U}(1)_Y$, where the subscript L stands for “left-handed” and the
249 subscript Y stands for “weak hypercharge”. Again, these subscripts indicate the types
250 of objects to which the corresponding gauge fields couple. For example, the gauge
251 fields of $\text{SU}(2)_L$ only couple to left-handed objects, and the gauge fields of $\text{U}(1)_Y$
252 only couple to weakly hypercharged objects. Initially, there are four massless gauge
253 fields in the electroweak theory ¹¹. After the spontaneous symmetry breaking of the
254 Higgs mechanism [41], these fields mix to give rise to three massive gauge fields and
255 one massless gauge field. The three massive gauge fields correspond to the familiar
256 W^\pm and Z^0 bosons, which are the mediating bosons of the weak interaction. The
257 massless gauge field corresponds to the photon, which mediates the electromagnetic
258 interaction.

¹¹Three corresponding to the generators of $\text{SU}(2)$, one corresponding to the generator of $\text{U}(1)$.

259 **1.2.2 The scalar sector**

260 The scalar sector of the Standard Model is quite lonely, and only corresponds to
261 one spin-zero field: the Higgs [41]. As mentioned in the previous section, the Higgs
262 mechanism that corresponds to this field is responsible for the acquisition of mass
263 by the W^\pm and Z^0 bosons. The Higgs field also couples to all of the fermions in the
264 Standard Model, but the mass acquisition procedure is *slightly* different¹² from the
265 massive bosons. The associated Higgs boson was discovered by the A Toroidal LHC
266 Apparatus (ATLAS) and Compact Muon Solenoid (CMS) collaborations in 2012 [45],
267 [46], and was the last major piece of the Standard Model to be experimentally verified.

268 **1.2.3 The fermionic sector**

269 The fermionic sector contains all of the spin one-half particles (quarks and leptons) in
270 the Standard Model. It is often convenient to group these particles into three genera-
271 tions, where each generation is identical except for the masses of the particles. It is
272 even *more* convenient to group the fermions within each family into multiplets, where
273 the members of the multiplet are related to each other by transformations within the
274 gauge group of the Standard Model (Equation 1.1). In other words, the fermions
275 within a particular multiplet can only be transformed to fermions within the same
276 multiplet. A table of the fermions in the Standard Model and their corresponding
277 multiplets can be seen in Table 1.1. The indices L and R correspond to the chirality
278 of the fields, and the indices r , g , and b represent the color charge of the fields. The
279 color charges are only non-zero for the quarks, making them the only fermions that
280 couple to the gauge fields of the strong interaction (gluons).

281 **1.3 Quantum chromodynamics**

282 Quantum chromodynamics (QCD) is the component of the Standard Model that
283 describes the strong interaction between quarks and gluons, the fundamental particles
284 that make up most of the matter in the universe. In this theory, the fermionic quarks
285 have “color charge”, which can either be red, green or blue for quarks, or anti-red,
286 anti-green, or anti-blue for anti-quarks. The gluons, which are the mediating bosons

¹²It’s still spontaneous symmetry breaking, but within the Yukawa part of the electroweak La-
grangian.

Table 1.1: The fermions of the Standard Model for each generation and their corresponding multiplets. The Standard Model does not allow for fermions to leave their respective multiplets.

Gen.	Left-handed quarks	Right-handed up quarks	Right-handed down quarks	Left- handed leptons	Right- handed leptons
1 st gen.	$\begin{pmatrix} u_L^r & u_L^g & u_L^b \\ d_L^r & d_L^g & d_L^b \end{pmatrix}$	$(u_R^r \ u_R^g \ u_R^b)$	$(d_R^r \ d_R^g \ d_R^b)$	$\begin{pmatrix} \nu_{eL} \\ e_L \end{pmatrix}$	(e_R)
2 nd gen.	$\begin{pmatrix} c_L^r & c_L^g & c_L^b \\ s_L^r & s_L^g & s_L^b \end{pmatrix}$	$(c_R^r \ c_R^g \ c_R^b)$	$(s_R^r \ s_R^g \ s_R^b)$	$\begin{pmatrix} \nu_{\mu L} \\ \mu_L \end{pmatrix}$	(μ_R)
3 rd gen.	$\begin{pmatrix} t_L^r & t_L^g & t_L^b \\ b_L^r & b_L^g & b_L^b \end{pmatrix}$	$(t_R^r \ t_R^g \ t_R^b)$	$(b_R^r \ b_R^g \ b_R^b)$	$\begin{pmatrix} \nu_{\tau L} \\ \tau_L \end{pmatrix}$	(τ_R)

287 of the strong interaction, also carry color charge, but in the form of a superposition of
 288 both color and anti-color. This section will delve into the details of QCD, emphasizing
 289 the properties of the strong interaction that make it so challenging to study.

290 1.3.1 The QCD Lagrangian

The dynamics of the Standard Model fields and how they interact are completely encoded within the Lagrangian of the theory, which can be used to calculate experimental observables like cross-sections and decay rates. However, the Lagrangian of the Standard Model is fairly long [47], and often not particularly insightful when trying to study a specific aspect of the theory. As such, when studying QCD, it is often useful to throw away the electroweak gauge fields, leptons, and scalars to look at only the QCD Lagrangian [48],

$$\mathcal{L}_{QCD} = -\frac{1}{4}F_{\mu\nu}^A F^{A\mu\nu} + i\bar{q}\gamma^\mu \left(\partial_\mu + ig_s \frac{1}{2}\lambda^A \mathcal{A}_\mu^A \right) q - \bar{q}_R \mathcal{M} q_L - \bar{q}_L \mathcal{M}^\dagger q_R - \theta\omega,$$

291 where all repeated indices are summed over.

292 The gluons are described by the vector gauge field \mathcal{A}_μ^A , with index A representing
 293 one of the eight color labels. These eight components belong to the color group
 294 $SU_c(3)$, which is the gauge group of QCD. The corresponding coupling constant is
 295 g_s , and the field strength tensor $F_{\mu\nu}^A$ is given by

$$F_{\mu\nu}^A = \partial_\mu \mathcal{A}_\nu^A - \partial_\nu \mathcal{A}_\mu^A + g_s f^{ABC} \mathcal{A}_\mu^B \mathcal{A}_\nu^C, \quad (1.2)$$

296 where f^{ABC} are the structure constants [49] of $SU_c(3)$. Note that while this field
 297 strength tensor shares the same letters as the electromagnetic field strength tensor
 298 $F_{\mu\nu}$, the additional term $g_s f^{ABC} \mathcal{A}_\mu^B \mathcal{A}_\nu^C$ in Equation 1.2 separates QCD and QED in a
 299 very fundamental way: the gluons are allowed to self-interact. This self-interaction is
 300 a direct result of the non-vanishing structure constants of $SU_c(3)$ ¹³, and is responsible
 301 for the challenging nature of QCD calculations.

302 The quarks are represented by the field q , where the color, flavor and spin indices
 303 have been suppressed. In reality, the quark field q has:

- 304 • six flavor indices $\{u, d, s, c, b, t\}$,
- 305 • four spin indices $\{0, 1, 2, 3\}$, and
- 306 • three color indices $\{r, g, b\}$,

307 where all of these indices are being implicitly summed over in \mathcal{L}_{QCD} . Luckily, all of
 308 the matrices $(\mathcal{A}_\mu^A, \lambda^A, \mathcal{M}, \gamma^\mu)$ act on separate sets of indices¹⁴. For example, the γ^μ s
 309 only operate on the spin indices, whereas both the gluon fields \mathcal{A}_μ^A and Gell-Mann
 310 matrices [15] λ^A operate on the color indices. These Gell-Mann matrices are the
 311 generators of $SU_c(3)$ and satisfy the commutation relation

$$[\lambda^A, \lambda^B] = 2i f^{ABC} \lambda^C. \quad (1.3)$$

312 The chiral quark fields q_L and q_R are defined as $\frac{1}{2}(1-\gamma_5)q$ and $\frac{1}{2}(1+\gamma_5)q$, respectively.
 313 The mass matrix \mathcal{M} operates on the flavor indices, and its form depends on the choice
 314 of basis for the quark fields [48]. It is often convenient to choose a basis where the
 315 mass matrix is diagonal, which can be done by independent rotations of q_L and q_R in
 316 $SU(6)$. Doing so gives the more familiar term

$$-\bar{q}_R \mathcal{M} q_L - \bar{q}_L \mathcal{M}^\dagger q_R = - \sum_{f=1}^6 \bar{q}_f m_f q_f, \quad (1.4)$$

317 where m_f is the mass of the quark with flavor f , and q_f is the flavor component of
 318 the quark field. Note that this term completely violates the $SU(2) \times U(1)$ electroweak
 319 symmetry, indicating that the given \mathcal{L}_{QCD} is determined *after* the spontaneous sym-
 320 metry breaking described in the previous section.

¹³Structure constants of Abelian gauge groups like $U(1)$ are trivially zero.

¹⁴Really the components of the field corresponding to those indices.

These quark masses are also subject to **renormalization** [50], which is a process that removes the infinities that arise from the self-interaction of the quarks and gluons. The renormalization process results in the running of the quark masses with respect to the energy scale μ of the interaction¹⁵. More simply, the quark masses are inversely dependent on this energy scale: at large μ , the quark masses are small, and at lower μ , the quark masses are large. At the energy scale $\mu \approx 2 \text{ GeV}$ (close to the mass of the proton), the masses of the up, down, and strange quarks—collectively referred to as the light-flavor quarks—are approximately $2.2 \text{ MeV}/c^2$, $4.7 \text{ MeV}/c^2$, and $96 \text{ MeV}/c^2$, respectively [52]. The heavy-flavor charm, bottom, and top quarks have masses of approximately $1.28 \text{ GeV}/c^2$, $4.18 \text{ GeV}/c^2$, and $173 \text{ GeV}/c^2$, respectively¹⁶.

The final term, known as the θ -term [53], is something of a mystery. It is a scalar term that violates CP symmetry [54], and is often set to zero as there is no experimental evidence for its existence. However, it is not clear why this term is zero, as there is no symmetry that explicitly forbids it. This is known as the **strong CP problem**, and is one of the biggest open questions in particle physics [55].

1.3.1.1 Brief aside: Why eight gluons?

The gluon field \mathcal{A}^A transforms under the adjoint representation of $SU(3)$, which is a representation of $SU(3)$ on the vector space of its Lie algebra $\mathfrak{su}(3)$. As $\mathfrak{su}(3)$ has eight basis elements (for instance, the Gell-Mann matrices λ^A from above), the adjoint representation of $SU(3)$ is eight-dimensional. Thus the gluon field has eight independent components, or, equivalently, there are eight gluons. In principle, QCD could have been built on top of a $U(3)$ gauge group, which would give rise to nine gluons (as the dimension of $U(n)$ is n^2). However, the singlet state in $U(3)$ would be required to be non-interacting; if it were, color neutral baryons would interact with each other via the strong interaction at a much longer range [56]. Such interactions have not been observed [57]. As there is no physical difference between $U(3)$ with a non-interacting singlet and $SU(3)$, the simpler gauge group was chosen.

¹⁵They also depend on the *choice* of renormalization scheme, with the most commonly implemented one being minimal subtraction or MS [51].

¹⁶At the energy scale governed by their respective masses (i.e. $\mu = m_Q$). [52]

348 **1.3.2 Properties of QCD**

349 **1.3.2.1 Confinement**

350 One of the unique properties of QCD is the phenomenon of **confinement**, which is
351 the observation that quarks and gluons are never seen in isolation. Instead, they are
352 *confined* inside of the color neutral bound states known as hadrons. This property
353 is mostly understood in terms of the coupling constant g_s . The renormalization [58]
354 of QCD gives rise to a g_s that varies with energy scale or distance. As the distance
355 between two quarks increases, so too does g_s . At some point, the coupling becomes so
356 strong that the energy required to separate the quarks is enough to create a quark-
357 anti-quark pair from the vacuum. Thus any attempts to separate a quark from a
358 hadron will always result in the creation of a new hadron, making it impossible to
359 observe single quarks in isolation.

360 The large coupling constant in this low energy regime makes it impossible to
361 describe this phenomenon using perturbative techniques, so the exact mechanism of
362 confinement is still not fully understood. However, it is often described using the
363 phenomenological Lund string model [59]. In this model, the field lines of two quarks
364 are pulled together due to the self-interaction of the gluons. This creates a string-like
365 structure between the two quarks, with a potential given by

$$V(r) \approx -\frac{4}{3} \frac{\alpha_s}{r} + \kappa r, \quad (1.5)$$

366 where r is the distance between the two quarks, $\alpha_s = \frac{g_s^2}{4\pi}$ and κ is the string tension.
367 This can be contrasted with the potential between two electrically charged particles,
368 where the field lines are not pulled together and become less dense as the distance
369 between the two particles increases. As such, the potential decreases with increasing
370 distance, opposite to that of the Lund model. A schematic of these differences can
371 be seen in Figure 1.4.

372 **1.3.2.2 Asymptotic freedom**

373 Just as the coupling constant becomes large at low energies and large distances, it
374 also becomes small at high energies and small distances. This property is known
375 as **asymptotic freedom**: at high enough energies, the quarks and gluons can be
376 thought of as “free”, and their interactions can be modeled using perturbative QCD

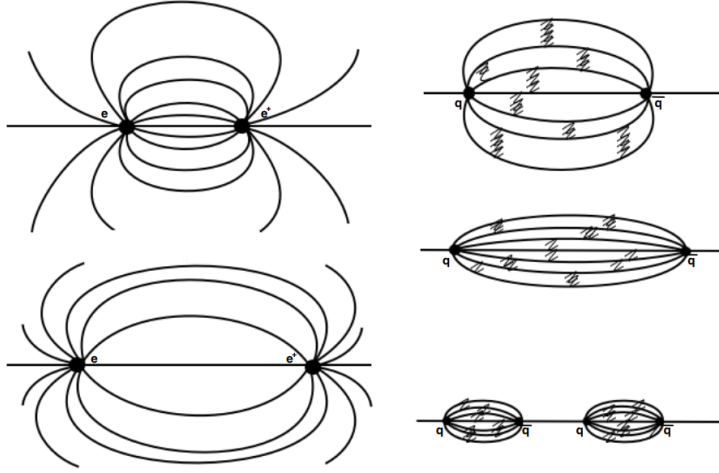


Figure 1.4: A schematic of the field lines between two electrically charged particles (left) and two quarks (right). The field lines between the quarks are pulled together due to the self-interaction of the gluons, whereas the electric field lines are not.

377 (pQCD). As discussed in Section 1.1, the discovery of asymptotic freedom in QCD was
 378 what allowed for the accurate predictions of the results of high energy particle collision
 379 experiments like SLAC [60] and PETRA [37]. The results of such experiments have
 380 also been used to calculate the value of the coupling constant itself at different energy
 381 scales, as shown in Figure 1.5. The value of α_s at the Z^0 mass is also given in the
 382 figure, which is the most accurate measurement of α_s to date [52].

383 1.3.2.3 Chiral symmetry breaking

384 The mass term in the QCD Lagrangian,

$$-\bar{q}_R \mathcal{M} q_L - \bar{q}_L \mathcal{M}^\dagger q_R, \quad (1.6)$$

385 explicitly breaks **chiral symmetry**: swapping the left-handed and right-handed com-
 386 ponents of the quark fields does not leave the Lagrangian invariant. The breaking of
 387 chiral symmetry due to the non-zero quark masses is referred to as **explicit** chiral
 388 symmetry breaking.

389 However, even in the limit of massless quarks, chiral symmetry is broken by the
 390 QCD vacuum. This is known as **spontaneous** chiral symmetry breaking, and due

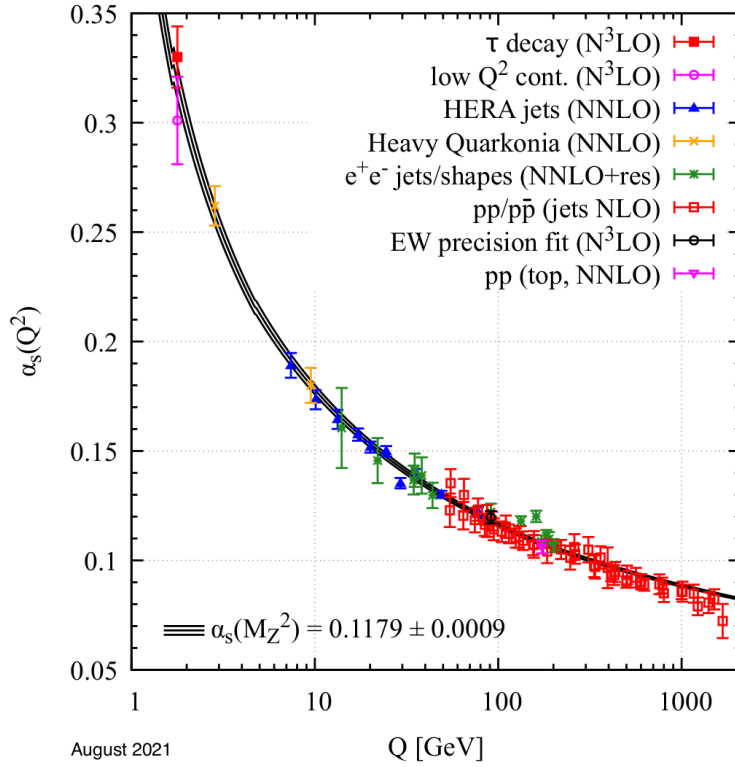


Figure 1.5: The value of the strong coupling constant α_s as a function of momentum transfer Q , which represents the energy scale of the interaction.

391 to the non-zero vacuum expectation value of the quark condensate [61]

$$\langle \bar{q}q \rangle = \langle \bar{q}_L q_R + \bar{q}_R q_L \rangle \neq 0. \quad (1.7)$$

392 This non-zero value is a direct result of the confinement of QCD **TongGaugeTheory**
 393 (Section 1.3.2.1), and implies that the ground state of the theory is filled with quark-
 394 anti-quark pairs. The spontaneous breaking of chiral symmetry in QCD gives rise
 395 to eight massless Nambu-Goldstone bosons **NambuGoldstone**, which are the pseu-
 396 doscalar mesons $\pi^{\pm,0}$, $K^{\pm,0}$, η , and η' . These mesons then acquire a small mass due
 397 to the aforementioned explicit chiral symmetry breaking from the quark masses.

398 **1.3.2.4 Jets**

399 During high energy particle collisions (between two protons, for example), the con-
 400 stituent partons of the protons will sometimes scatter off each other in a way that con-

verts most of their initial longitudinal momentum (along the collision axis) into transverse momentum (in the plane perpendicular to the collision axis). Such a scattering is often referred to as a **hard scattering**. Because the momentum transfer is large, the cross-section of the parton-parton scattering is calculable using pQCD. Furthermore, branching processes of the high momentum partons—like gluon radiation—can also be calculated perturbatively. Eventually, however, the partons will lose enough energy such that their behavior can no longer be described using perturbative techniques.

Luckily, the aforementioned Lund model is well-equipped to deal with lower energy partons. Under the Lund model, as these colored partons move away from each other, the force between them increases until there is enough energy to produce a quark-anti-quark pair (as discussed in Section 1.3.2.1). This process—known as string fragmentation—continues until the partons are no longer energetic enough to move away from each other, at which point they hadronize into a large number of color neutral bound states. These particles are roughly collimated in the direction(s) of the initial hard scattering, forming sprays of hadrons known as **jets**. A diagram depicting the formation of a jet from an initial hard scattering of partons can be seen in Figure 1.6.

1.3.2.5 Flavor conservation

One interesting feature of the interactions in QCD is that all **flavor** quantum numbers are conserved. Specifically, the number of quarks minus the number of anti-quarks of each flavor is a conserved quantity in every strong interaction¹⁷. In this thesis, the most important flavor quantum number is **strangeness**, which is defined as

$$S = -(n_s - n_{\bar{s}}), \quad (1.8)$$

where n_s is the number of strange quarks and $n_{\bar{s}}$ is the number of strange anti-quarks. The “minus” sign in front of the expression indicates that the strangeness of a strange quark is negative (-1), and the strangeness of a strange anti-quark is positive ($+1$).

¹⁷Conservation of the “historical” flavor quantum number *isospin* (from Section 1.1), which is $+\frac{1}{2}$ for up quarks and $-\frac{1}{2}$ for down quarks, is equivalent to the conservation of $n_{u,d} - n_{\bar{u},\bar{d}}$ when baryon number is considered. Baryon number is an absolutely conserved quantum number in the Standard Model [52], and (anti-)quarks have baryon number $(-)\frac{1}{3}$.

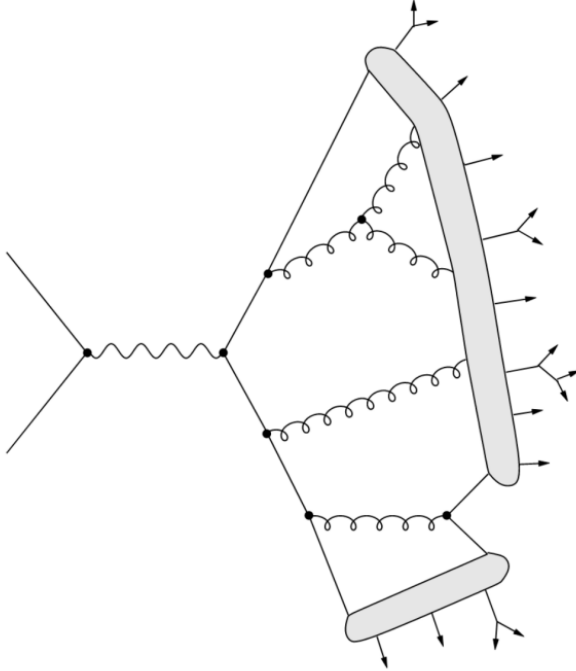


Figure 1.6: A diagram depicting the formation of a jet within the Lund model from an initial hard scattering of partons, adapted from [62]. The vertices represent perturbative QCD processes, the shaded regions represent string fragmentation/hadronization, and the outgoing arrows represent the resulting hadrons (which may decay further).

427 This convention is chosen¹⁸ to make the signs of these “flavor charges” consistent
 428 with the signs of the electric charges of these quarks, which are $-\frac{1}{3}$ for the strange
 429 quark and $+\frac{1}{3}$ for the strange anti-quark. Strangeness conservation has an interesting
 430 consequence for particle collisions between atomic nuclei: as the total strangeness of
 431 these nuclei (protons and neutrons) is zero, the number of strange and anti-strange
 432 quarks produced from the strong interaction during these collisions must be equal.
 433 In other words, the production of strange quarks in these collisions must come in the
 434 form of strange quark-anti-quark ($s\bar{s}$) pairs.

¹⁸Really this is a historical convention that stems from the fact that “strangeness” was introduced as a concept before the existence of any quark models, as mentioned in Section 1.1.

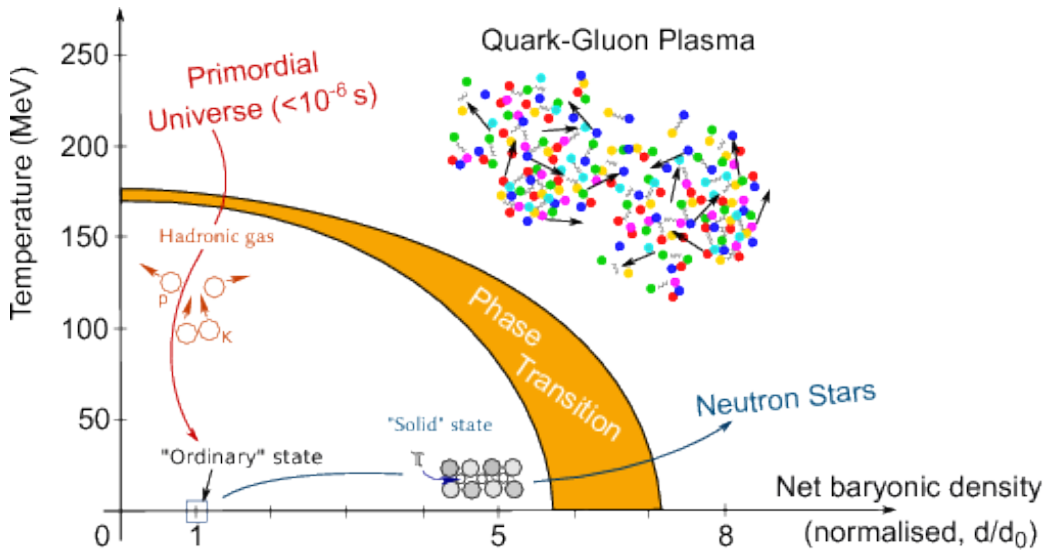


Figure 1.7: A phase diagram of the QGP, taken from [65]. The axes are temperature and baryon density, and the orange band represents the phase transition from normal hadronic matter to the QGP.

435 1.4 The Quark-Gluon Plasma

436 One of the consequences of the asymptotic freedom of QCD is the prediction of
 437 a new state of matter at extreme temperatures and densities: the **quark-gluon**
 438 **plasma** (QGP) [63], [64]. In this plasma, the quarks and gluons are not confined
 439 inside hadrons, and instead behave as quasi-free particles. This is analogous to an
 440 electromagnetic plasma, where electrons and protons are dissociated from their atoms.
 441 A phase diagram of this plasma can be seen in Figure 1.7. This diagram has two
 442 axes: temperature and baryon density. Increasing *either* of these quantities beyond
 443 a certain threshold will cause a phase transition from normal hadronic matter to the
 444 QGP. Similarities can be drawn between this phase diagram and that of a snowball:
 445 heating *or* squeezing a snowball will cause it to melt into a liquid¹⁹.

446 Numerical simulations of QCD on a lattice **LatticeQCD1**, **LatticeQCD2** (known
 447 as lattice QCD or lQCD) have shown that at zero baryon density, the transition from
 448 hadronic matter to the QGP occurs as a smooth crossover **LatticeQCD Crossover**
 449 with a critical temperature $T_C \approx 160$ MeV or 10^{12} K, 10,000 times hotter than the cen-

¹⁹Be careful: if you continue to heat up the snowball enough, or squeeze hard enough, it will undergo another phase transition into the QGP.

450 ter of the sun. LQCD has also been used to predict the existence of a critical endpoint
451 in the QGP phase diagram at a non-zero baryon density **LatticeQCD.CriticalPoint**,
452 beyond which the transition from hadronic matter to the QGP is no longer a smooth
453 crossover, but a first-order phase transition. However, due to the complex action
454 problem **ComplexActionProblem**, lQCD simulations at non-zero baryon density
455 are not yet possible²⁰. Thus the exact location of this critical endpoint is still un-
456 known, and is the subject of much experimental and theoretical research [66].

457 As the temperatures at the early stages of the universe were well beyond the
458 critical temperature predicted by lQCD, it is thought that the universe was filled
459 with a QGP in the first few microseconds after the Big Bang [66]. Thus studying the
460 QGP is of interest to cosmologists, as it can give insight to the early universe and
461 its expansion, which is schematically represented in Figure 1.8. It is also postulated
462 that QGP formation occurs in the cores of neutron stars [67], giving another avenue
463 of interest for astrophysicists. Furthermore, studying the QGP and its properties can
464 help illuminate the dark, confounding corners of QCD that are not yet understood—
465 like confinement—making it an exciting subject of study for particle physicists. The
466 remainder of this section will discuss the theoretical characteristics of this interesting
467 plasma.

468 1.4.1 Properties of the QGP

469 1.4.1.1 Deconfinement

470 The most defining characteristic of the QGP is that the quarks and gluons within the
471 plasma are not confined inside hadrons, and instead interact as quasi-free particles. As
472 mentioned in Section 1.3.2.2, the coupling constant g_s becomes smaller with increasing
473 energies. At high enough energies, the coupling constant becomes small enough
474 that the quarks and gluons become deconfined. In lQCD, the order parameter for
475 deconfinement is the Polyakov loop expectation value **PolyakovLoop** $\langle L \rangle$, which
476 is zero in the confined phase and greater than zero in the deconfined phase. This
477 transition, from $\langle L \rangle = 0$ to $\langle L \rangle > 0$, is used²¹ to define the transition from hadronic

²⁰Though there are plenty of techniques to extend the lQCD results **TaylorSeries**, **ComplexDensity**, they are only applicable at small baryon densities.

²¹Technically the more common order parameter is the quark condensate discussed in the next section, but the critical temperatures predicted by lQCD using these different order parameters are usually very similar **QCDOOrderParameterSimilarity**.

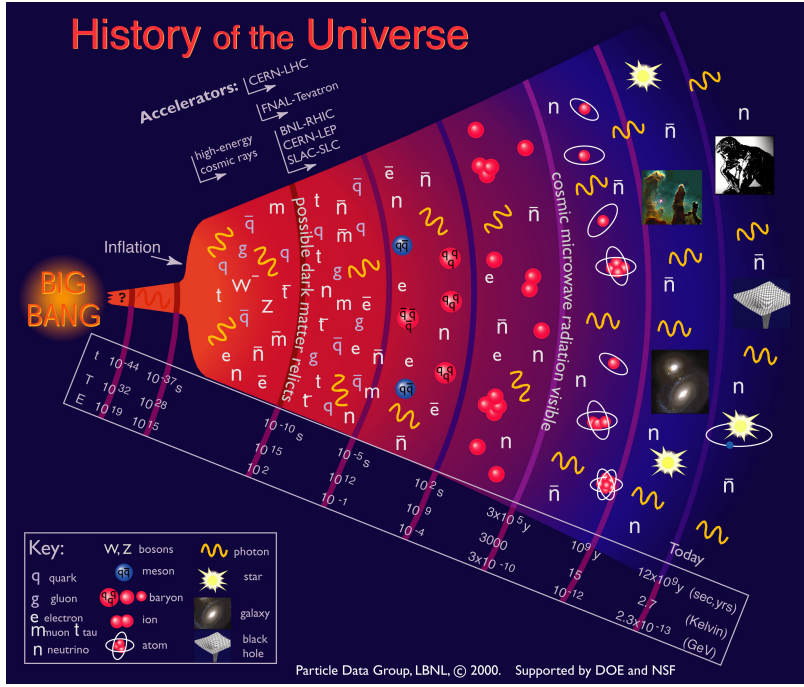


Figure 1.8: A schematic of the evolution of the universe, taken from [52]. The QGP phase of the universe on this diagram lies roughly between 10^{-10} and 10^{-5} seconds after the Big Bang.

478 matter to the QGP.

479 1.4.1.2 Chiral symmetry restoration

480 As mentioned in Section 1.3.2.3, the QCD vacuum has a non-zero quark condensate
 481 $\langle q\bar{q} \rangle$ which spontaneously breaks chiral symmetry. However, this non-zero condensate
 482 is the direct result of the confinement of QCD **TongGauge**. Thus, in the QGP—
 483 where the quarks and gluons are no longer confined—the quark condensate should
 484 vanish. As such, another defining characteristic of the QGP is the restoration of the
 485 spontaneously broken chiral symmetry of QCD, often referred to as **chiral symmetry**
 486 **restoration**. This transition, from $\langle q\bar{q} \rangle > 0$ to $\langle q\bar{q} \rangle = 0$, is also used to define the
 487 QGP phase transition.

488 An lQCD diagram of the deconfinement order parameter $\langle L \rangle$ and chiral symmetry
 489 order parameter $\langle q\bar{q} \rangle$ (along with their corresponding susceptibilities) as a function
 490 of the coupling $\beta = 6/g_s^2$ can be seen in Figure 1.9. Note that the susceptibilities
 491 are maximal at the same coupling value (corresponding to a critical temperature of

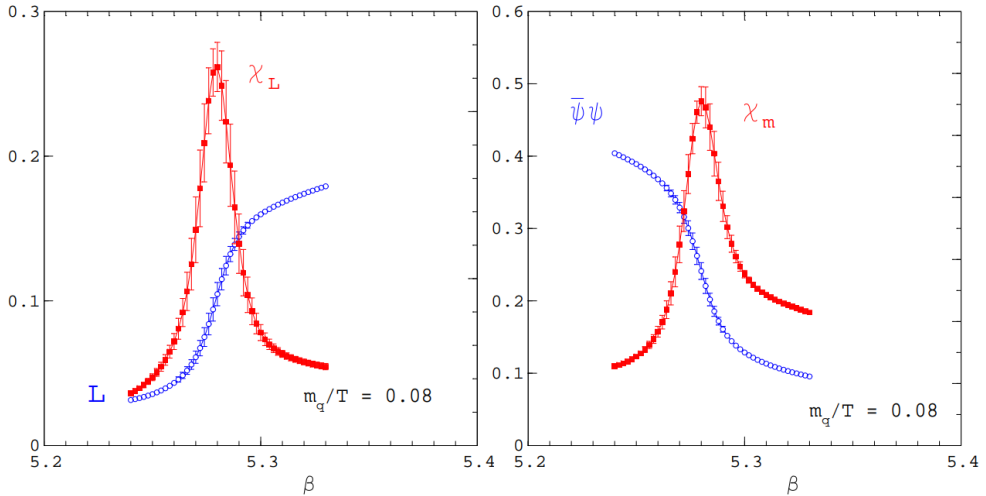


Figure 1.9: The deconfinement order parameter $\langle L \rangle$ and chiral symmetry order parameter $\langle q\bar{q} \rangle$ (along with their corresponding susceptibilities) as a function of the coupling $\beta = 6/g_s^2$ using 2-flavor 1QCD, taken from **FrithofLattice**. The critical temperatures (indicated by the maxima of the susceptibilities) occur at roughly $\beta = 5.28$, corresponding to a temperature of around 170 MeV.

around 170 MeV), indicating that both deconfinement and chiral symmetry restoration correspond to the same phase transition, namely the transition from hadronic matter to the QGP.

1.4.1.3 Hydrodynamic behavior

The QGP is a strongly interacting plasma. As such, it is expected to exhibit fluid-like behavior at a macroscopic level. Unfortunately, the calculation of QGP transport coefficients from first principles using QCD is very difficult **FlowViscPaper**. Using perturbative techniques to calculate the shear and bulk viscosities of the QGP results in values that are an order of magnitude larger than those extracted from experimental data **Visc1**, **Visc2**. The extraction of these transport coefficients using 1QCD is also challenging, as the aforementioned complex action problem makes it nearly impossible to simulate the QGP at non-zero baryon density. The most promising approach to calculating these transport coefficients is through the use of the AdS/CFT correspondence **AdSCFT**, which is a duality between a strongly coupled gauge theory (like QCD) and a weakly interacting gravitational theory (like string theory **StringTheory**). This approach has been used to approximate the

508 lower bound of the shear viscosity of a strongly-coupled medium **QGPViscADS**,

$$\eta/s \approx 1/4\pi, \quad (1.9)$$

509 which is often described as the shear viscosity of a “perfect fluid” **PerfectFluid**.
510 Experimental evidence suggests that the QGP has a shear viscosity that is very close
511 to this lower bound **QGPViscExp**, indicating that it is a nearly perfect fluid.

512 1.4.1.4 Radiative energy loss

513 Partons traveling through the QGP lose energy through both collisional and radiative
514 processes, as shown in Figure 1.10. The collisional energy loss is due to elastic
515 scattering between the partons and the constituents of the QGP. For a parton with
516 energy E much greater than its mass and the temperature of the QGP, the collisional
517 energy loss is given by **GluonRadiation**

$$\Delta E_{\text{coll}} \sim \alpha_s^2 T^2 L, \quad (1.10)$$

518 where T is the temperature of the QGP and L is the length of travel through the
519 medium (which is assumed to be larger than the critical length $L_{cr} \sim \frac{1}{\alpha_s T} \sqrt{\frac{E}{T}}$).
520 The radiative energy loss is due to gluon radiation induced by the presence of the
521 medium²². Again, for a parton with $E \gg M, T$, the radiative energy loss is given
522 by **GluonRadiation**

$$\Delta E_{\text{rad}} \sim \alpha_s^2 \sqrt{ET^3} L, \quad (1.11)$$

523 where E is the energy of the parton. As the radiative energy loss is proportional
524 to \sqrt{E} , it is the dominant energy loss mechanism for light, energetic partons (i.e.
525 u , d , and s quarks as well as gluons). However, gluons lose more energy than the
526 light quarks due to their larger color charge. The heavier quarks are expected to
527 lose less energy through radiative processes due to the *dead cone effect*, whereby the
528 gluon radiation is suppressed in the forward direction due to the larger masses of the
529 heavy quarks **DeadCone**. Even still, the radiative energy loss of heavy quarks is
530 larger than their collisional energy loss **DeadCone**, making radiative energy loss the
531 dominant energy loss mechanism for all energetic partons in the QGP.

²²Similar to bremsstrahlung, where electrically charged particles radiate photons in the presence of other charged particles.

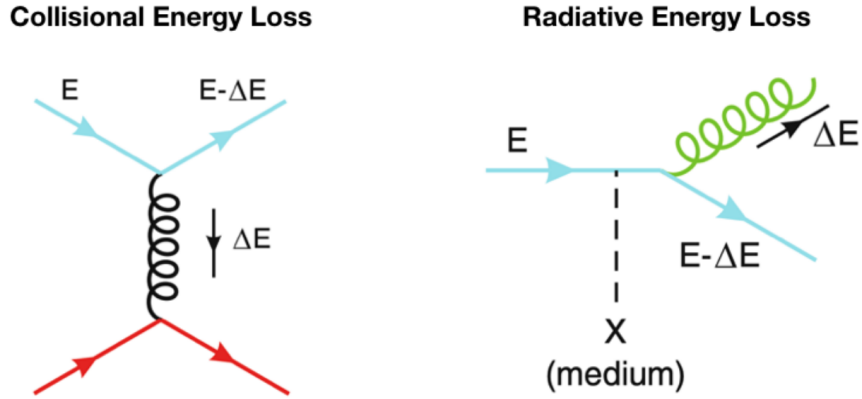


Figure 1.10: A diagram depicting the collisional (left) and radiative energy loss (right) processes of a parton traveling through the QGP. Radiative energy loss is the dominant energy loss mechanism for all energetic partons in the QGP.

532 1.4.2 Enhanced s -quark production

533 In the context of the research presented in this thesis, the most important characteristic
 534 of the QGP is the increase in the production of strange quarks relative to
 535 the production of up and down quarks [18]. Discovered in 1981 by physicists Johann
 536 Rafelski and Rolf Hagedorn, this *enhancement* in the production of strange quarks
 537 in the QGP is often referred to as **strangeness enhancement**. As mentioned in
 538 Section 1.3.2.5, strangeness is conserved during strong interactions. As such, the
 539 production of $s\bar{s}$ pairs can only come from four Feynman diagrams (to lowest order
 540 in pQCD), shown in Figure 1.11. A key insight made by Rafelski and Hagedorn is
 541 that in the QGP, the higher temperatures allow for the thermal production of $s\bar{s}$ pairs
 542 through gluon fusion ($gg \rightarrow s\bar{s}$ or diagrams (a) (b) and (c) in Figure 1.11). This gluon
 543 fusion occurs much faster than the quark-based production ($q\bar{q} \rightarrow s\bar{s}$ or diagram (d)
 544 in Figure 1.11), and allows for the full chemical equilibration of strangeness in the
 545 QGP in less than 10^{-24} seconds. Strangeness equilibration in a hadronic gas, on the
 546 other hand, takes much longer: on the order of 10^{-10} seconds [18].

547 1.4.2.1 Statistical hadronization

548 The production of strangeness in the QGP and within a hadron gas is often described
 549 in terms of the **statistical hadronization model** (SHM). The SHM is based off of

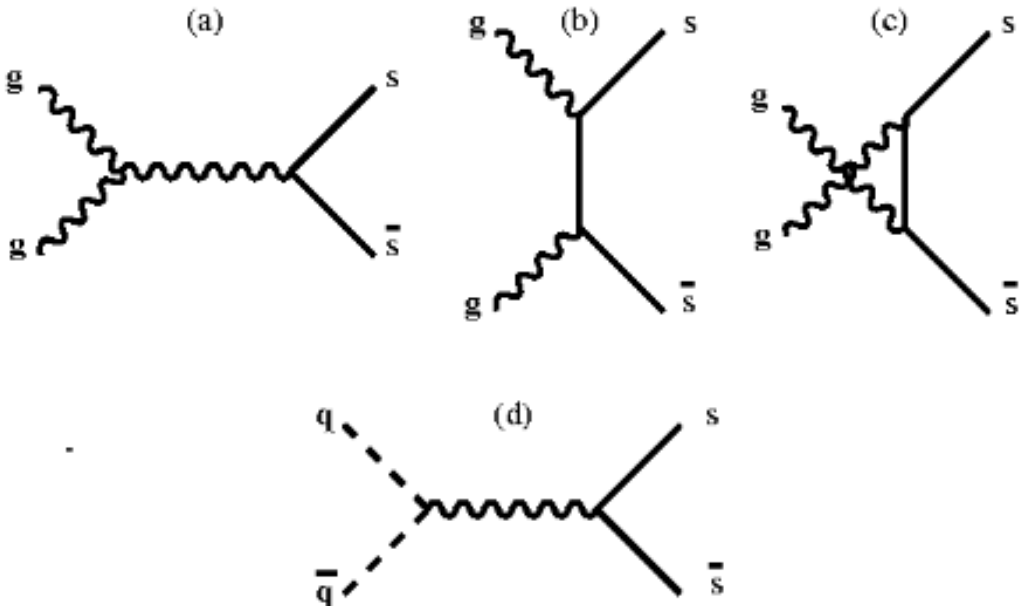


Figure 1.11: The four leading-order Feynman diagrams responsible for the production of $s\bar{s}$ pairs in the QGP, adapted from [18]. Diagrams (a), (b) and (c) are the gluon fusion processes, while diagram (d) is the quark-based process.

the Fermi model of hadron formation, where it is assumed that the strong interactions saturate the quantum particle production matrix elements **RafelskiStatisticalH**. This assumption allows for the calculation of the particle yields using only conservation laws and the available phase space, while ignoring the unknown microscopic details of the hadronization process. In the fundamental micro-canonical approach for the SHM, the available phase space is determined by the energy density of localized “clusters” within the system. However, a grand canonical framework for the SHM is often used for highly energetic systems, where the phase space is determined by a global temperature-like parameter T .

The most important quantity for describing particle yields within the grand canonical SHM is the particle fugacity λ_i , which is defined as

$$\lambda_i = e^{\mu_i/T}, \quad (1.12)$$

where μ_i is the chemical potential of particle i . In essence, the fugacity “counts” the number of particles of type i in the system [18]. For systems in absolute chemical equilibrium, the chemical potentials for particle and anti-particle flavors are opposite

564 to each other. Consequently, the relationship between the particle and anti-particle
 565 fugacities is given by

$$\lambda_{\bar{i}} = \lambda_i^{-1}. \quad (1.13)$$

566 However, this relationship does not hold for systems that have not reached absolute
 567 chemical equilibrium, as the chemical potentials of the particle and anti-particle fla-
 568 vors are no longer opposite to each other. Due to the higher mass of the strange
 569 quark, the production of $s\bar{s}$ pairs usually proceeds at a much slower rate than the
 570 production of $u\bar{u}$ and $d\bar{d}$ pairs. As such, obtaining absolute chemical equilibrium for
 571 strange particles is difficult, especially in hadronic matter²³.

572 To account for this, the SHM introduces the concept of *relative* chemical equilib-
 573 rium, in which the strange phase space is not fully saturated, but whatever strangeness
 574 is produced is distributed among the strange hadron channels according to the law
 575 of maximum entropy **9212210hepph**. The extent to which the strange phase space
 576 is saturated is parameterized by $0 < \gamma_s \leq 1$, which gives a modified particle fugacity,

$$\lambda_i^{\text{mod}} = \gamma_s^{n(i,s)} \lambda_i, \quad (1.14)$$

577 where $n(i, s)$ is the number of strange quarks plus the number of strange anti-quarks
 578 in particle i . The factor γ_s approaches unity whenever the strange phase space is fully
 579 saturated (i.e. when the system is in absolute chemical equilibrium). This factor can
 580 be determined by looking at strange particle ratios, which are sensitive to the value
 581 of γ_s . For example, the ratio of Λ baryons to protons is related to γ_s by

$$\gamma_s^2 = \frac{\Lambda}{p} \times \frac{\bar{\Lambda}}{\bar{p}}. \quad (1.15)$$

582 As these particle ratios can be measured by particle collision experiments, it is
 583 possible to determine the value of γ_s for a given collision system. Measuring γ_s in
 584 heavy-ion collisions is of particular interest, as it is believed that the QGP is formed
 585 in these collisions. However, heavy-ion collisions are very short-lived systems, lasting
 586 only around $10^{-23} - 10^{-22}$ seconds [68]. As mentioned previously, full chemical equi-
 587 libration in a hadronic gas cannot occur within this time frame. As such, measuring
 588 values of γ_s close to unity in heavy-ion collisions would be a strong indication of QGP
 589 formation.

²³As mentioned in the previous section, strangeness equilibration in a hadronic gas is over X times slower than in the QGP

590 **1.5 Using Heavy-Ion Collisions to Study the**
591 **QGP**

592 The QGP phase diagram in Figure 1.7 shows two methods for producing the QGP:
593 increasing the system's temperature or increasing its baryon density. Noteably, these
594 two methods are not mutually exclusive:

- 595 • Baryon density can be increased by looking at systems with a lot of baryons
596 packed together (like the nucleus of a lead atom)
- 597 • Temperature can be increased by smashing the aforementioned systems together
598 at higher energies (like in a particle accelerator)

599 Thus one of the best (and only) ways to study the QGP in a laboratory setting is
600 through relativistic **heavy ion collisions**: the smashing together of two heavy nuclei
601 at very high energies using a particle accelerator.

602 Unfortunately, producing the QGP in this manner has a major drawback; while
603 it is possible to heat up the system beyond the critical temperature required for
604 QGP formation, the system expands and cools *very* quickly. For example, the QGP
605 produced by colliding lead ions with center-of-mass energy $\sqrt{s_{NN}} = 2.76$ TeV at the
606 Large Hadron Collider (LHC) only lasts for around $3 \text{ fm}/c$ [68], or 10^{-23} seconds. A
607 diagram depicting the formation and evolution of the QGP in a heavy ion collision
608 can be seen in Figure 1.12. This diagram can be split up into the following stages:

- 609 1. The Lorentz-contracted nuclei approach each other at very high energies, and
610 the partons within the nuclei scatter off each other ($t = 0 \text{ fm}/c$).
- 611 2. As new partons are created from the initial scatterings, the energy density of
612 the system increases. Eventually this energy density is high enough to create
613 the QGP ($t \approx 1 \text{ fm}/c$).
- 614 3. Once the QGP is formed, it expands and cools in a hydrodynamic manner.
- 615 4. After the QGP cools below the critical temperature, the partons begin to
616 hadronize, resulting in the formation of a hadron gas ($t \approx 3 \text{ fm}/c$).

617 5. The hadron gas will continue to expand until the hadrons within the gas are no
618 longer strongly interacting with each other ($t \approx 10 \text{ fm}/c$). This is often broken
619 up into two stages:

- 620 • The hadrons cease to interact *inelastically*, called **chemical freeze-out**.
621 • The hadrons cease to interact *elastically*, called **kinetic freeze-out**.

622 6. If a detector is built within a few meters around the collision point, the final
623 state hadrons can be observed ($t \approx 10^{15} \text{ fm}/c$).

624 The last stage of this diagram is perhaps the most frustrating: it is only possible
625 to study the QGP by observing the final state hadrons. Luckily, there are some
626 key observables associated with those final state hadrons that can shed light on the
627 formation and evolution of this exciting plasma. Before those observables can be
628 discussed, however, it is necessary to introduce a key concept in heavy ion collisions:
629 the centrality of the collision.

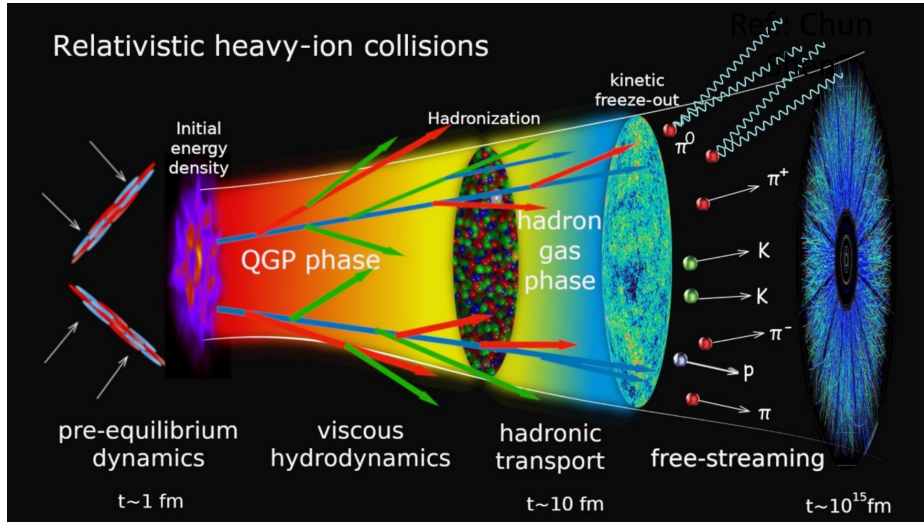


Figure 1.12: A schematic of the formation and evolution of the QGP in a heavy ion collision. The QGP is formed in the overlap region of the two colliding nuclei, and then expands and cools very quickly.

630 **1.5.1 Collision centrality**

631 The very first step of the heavy ion collision process involves the scattering of the
632 partons within the two nuclei. However, these nuclei are not point-like objects: they
633 have a finite size, and therefore need not collide “head-on”. Instead, the nuclei
634 can collide at different **impact parameters** (commonly denoted as b), as shown in
635 Figure 1.13. The impact parameter is defined as the distance between the centers
636 of the two nuclei, measured in the transverse plane (the plane perpendicular to the
637 initial directions of the nuclei). Collisions with a large impact parameter give rise to
638 *spectator* nucleons, which do not participate in the collision and continue traveling
639 as they please.

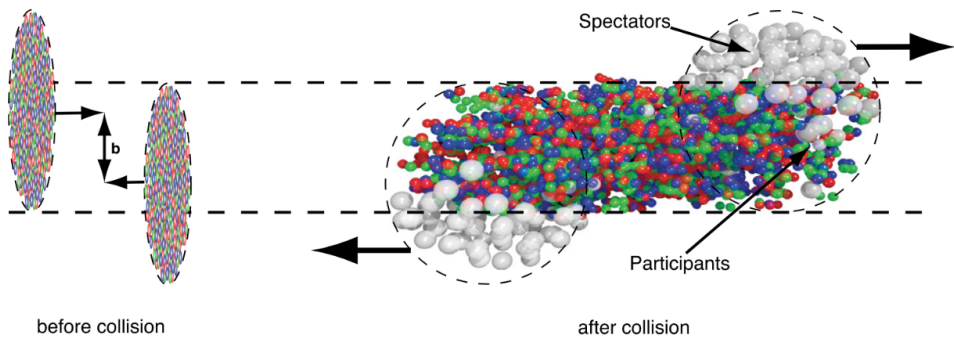


Figure 1.13: A schematic of a heavy ion collision with impact parameter b , taken from [69].

640 The impact parameter is very important when studying the QGP for a fairly
641 straightforward reason: as the impact parameter decreases, the number of partonic
642 scatterings increases, which in turn increases the energy density of the system. In
643 some sense, the size of the impact parameter determines whether or not the QGP is
644 formed in the subsequent stages of the collision. As such, characterizing heavy ion
645 collisions by their impact parameter is quite useful. Unfortunately, much like the
646 QGP, the impact parameter is not directly measurable and must be inferred from the
647 final state hadrons.

648 Instead of classifying collisions based off their unobtainable impact parameter,
649 they are instead classified by their **collision centrality**. The collision centrality is

650 defined as

$$c = \frac{\int_0^b d\sigma/db' db'}{\int_0^\infty d\sigma/db' db'} = \frac{1}{\sigma_{AA}} \int_0^b \frac{d\sigma}{db'} db', \quad (1.16)$$

651 where σ_{AA} is the total cross section of the nucleus-nucleus (A-A) collision. As this
652 number is strictly between 0 and 1, it is often expressed as a percentile: 0% corre-
653 sponds to the most central collisions (lowest impact parameters), and 100% corre-
654 sponds to the most peripheral collisions (highest impact parameters). If a monotonic
655 relationship between b and the number of final state particles seen in the detector is
656 assumed, the collision centrality can be experimentally determined [70]. The number
657 of final state particles from a collision is called the **multiplicity** of the collision, and
658 is often denoted as N_{ch} . The subscript ch indicates that only charged particles are
659 counted, as neutral particles are not seen by most detectors.

660 In practice, the collision centrality percentiles are usually determined by looking
661 at the distribution of events as a function of the signal (effectively N_{ch}) as measured
662 by a particular detector. The percentile for a specific event can then be determined
663 by integration:

$$c \approx \frac{1}{\sigma_{AA}} \int_{N_{ch}}^\infty \frac{d\sigma}{dN'_{ch}} dN'_{ch}, \quad (1.17)$$

664 where N_{ch} is the multiplicity of the event in question. An example of separating
665 events into centrality percentiles using this method can be seen in Figure 1.14. In
666 this plot, Pb-Pb collisions are characterized by their event activity in the ALICE
667 VZERO detector (which will be discussed in more detail in the next chapter). The
668 red points correspond to fits obtained using Monte Carlo simulations based off of the
669 Glauber model [70], [71]. The Glauber model [72] is a geometric model that treats
670 the nuclei as a collection of nucleons, and models the collisions as a superposition of
671 binary nucleon-nucleon collisions. This model gives a relationship between the impact
672 parameter b , the number of participating nucleons N_{part} , and the number of binary
673 nucleon-nucleon collisions N_{coll} . While not of particular import to this thesis, fitting
674 the Glauber model to the data actually allows for the determination of the impact
675 parameter corresponding to a given multiplicity percentile. The fact that the model
676 describes the data well also serves as a sanity check for the experimental estimation
677 of the collision centrality. In this thesis, the terms “multiplicity percentile” and
678 “collision centrality” will be used interchangeably.

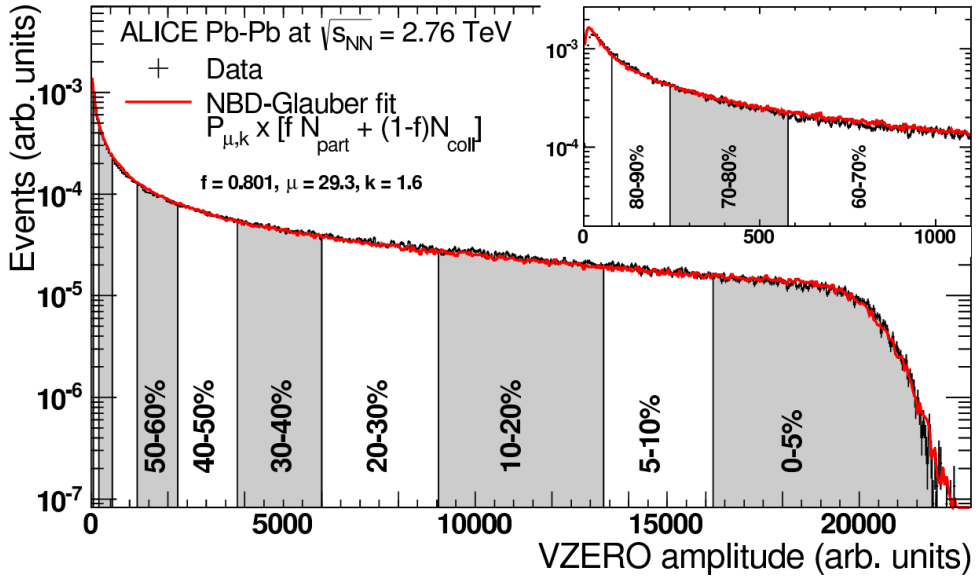


Figure 1.14: The distribution of Pb–Pb collision events as a function of event activity in the ALICE VZERO detector, taken from [71].

679 The approximation given by Equation 1.17 has an additional benefit: it allows
 680 for the determination of centrality without a clearly defined impact parameter. This
 681 is useful for proton-proton and proton-lead collisions, where the impact parameter is
 682 ill-defined.

683 1.5.2 Experimental evidence for QGP formation

684 As mentioned in Section 1.5, the QGP produced within a heavy ion collision is *very*
 685 short lived. As such, any attempt to study the QGP and its formation must be
 686 done using the detector-accessible final state hadrons. Luckily there are a number of
 687 signatures that can be used to study the QGP in experiment, including

- 688 • **jet quenching** [73], where the energy of a jet is heavily reduced due to its
 689 interactions with the QGP,
- 690 • **collective flow** [74], where the motion of the partons within the QGP is heavily
 691 influenced by the overall fluid-like medium, and

- 692 • **strangeness enhancement** [18], where the QGP exhibits an increase in the
693 production of strange quarks relative to up and down quarks.

694 These signatures are discussed in more detail in the following sections.

695 1.5.3 Jet quenching

696 The high momentum partons produced in the initial hard scatterings of heavy ion
697 collisions often traverse the QGP medium. Much like electron tomography, where the
698 passage of electrons through an atomic medium can give insight to the structure of the
699 atoms within, these high momentum partons can be used to probe the QGP. These
700 colored partons interact with the colored medium, losing energy in the process. As
701 discussed in Section 1.3.2.4, these partons are never observed individually; instead,
702 they hadronize into a spray of particles known as a jet. Thus the energy lost by
703 the parton is not observed directly, but rather as a reduction in the energy of the
704 resulting jet. This phenomenon is known as **jet quenching**, and is one of the most
705 well studied signatures of QGP formation.

706 Experimentally, this quenching is observed by studying *dijets*. While the term
707 “jet” refers to a single spray of particles observed in the detector, the initial hard
708 scattering responsible for the formation of the jet corresponds to the production of
709 *two* high momentum partons. Traveling in opposite directions in the transverse plane,
710 these partons often produce two jets that are back-to-back in φ (the azimuthal angle
711 in the transverse plane). These two jets are collectively referred to as a dijet. In pp
712 collisions, the energy of the two jets is roughly equal as the corresponding partons
713 don’t lose energy to a medium. In heavy ion collisions, however, the partons lose
714 energy to the QGP due to gluon radiation and elastic scattering with the medium’s
715 constituents [75]. If one of the two partons has a larger path length through the
716 QGP, it will lose more energy than the other parton, resulting in an imbalance in the
717 energy of the two jets. A schematic of this process for pp and A–A collisions can be
718 seen in Figure 1.15.

719 However, the path length within the QGP of the dijet-forming partons should be
720 roughly uniform, washing out this assymetry over a large event sample. As such, jet
721 quenching is experimentally observed by selecting high momentum “trigger” hadrons,
722 which most likely originated from the parton with the smaller QGP path length. The
723 jet corresponding to this higher momentum trigger—referred to as the “near-side” jet—

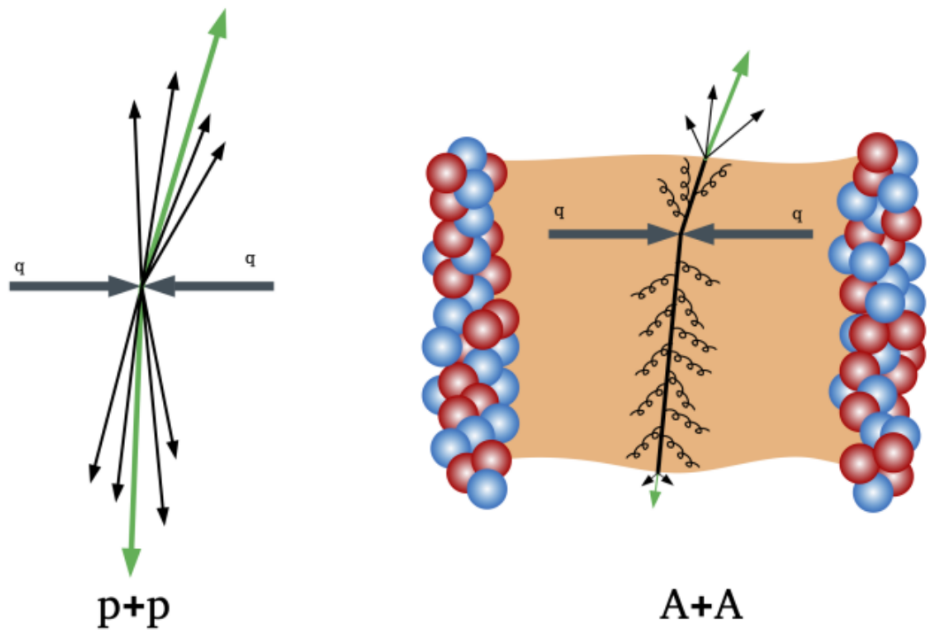


Figure 1.15: A schematic of the formation of dijets in $p+p$ and $A-A$ collisions, taken from [76].

is then compared with its partner jet, which would be 180° away in azimuth—called the “away-side” jet. The first collaboration to observe this jet quenching was the STAR collaboration at the Relativistic Heavy Ion Collider (RHIC) [77]. By looking at high transverse momentum hadrons produced in Au–Au collisions, they found that the away-side jet began to “disappear” as the centrality of the collision increased, as shown in Figure 1.16. This disappearance is due to the away-side jet losing energy to the QGP, such that the corresponding hadrons in the away-side fall below the momentum cutoff.

1.5.4 Collective flow

The QGP is a strongly interacting medium, whose constituent partons are heavily coupled to their surroundings. Just as the pebbles within a river get swept up in the flow of the water, the partons within the QGP are influenced by the flow of this medium. This flow manifests itself by the presence of collective effects in the final state hadrons, which are often quantified using **collective flow** components. These

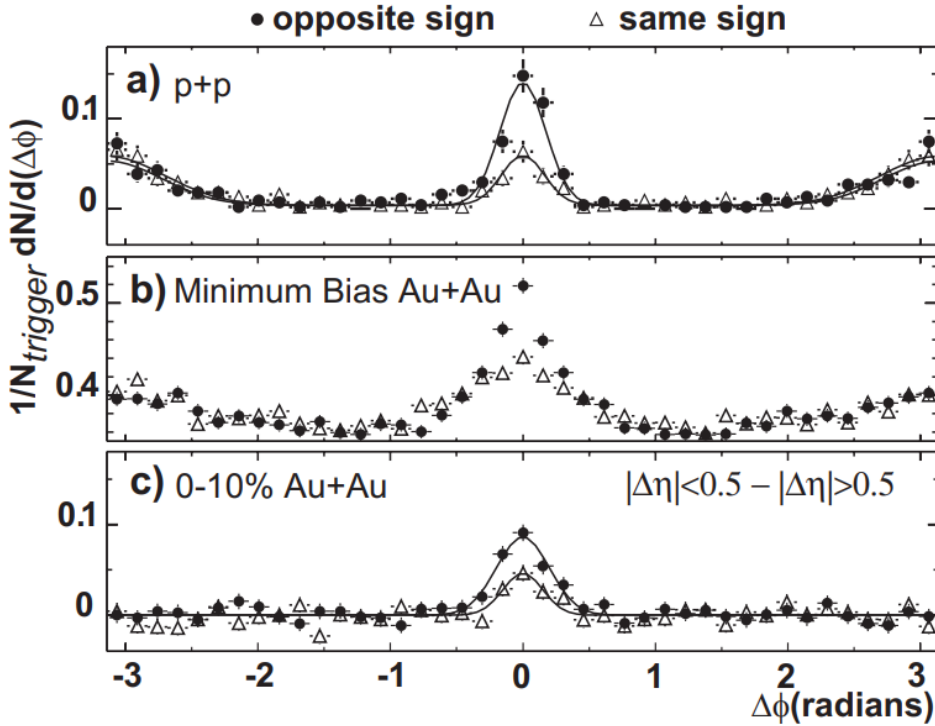


Figure 1.16: Hadron yields corresponding to the near-side jet (near $\Delta\varphi = 0$) and the away-side jet ($\Delta\varphi = \pm\pi$), taken from [77]. In pp and minimum bias Au–Au collisions, the away-side jet is present. However, at high centrality (0–10%), the away-side jet completely disappears.

738 flow components are obtained by expanding the final state hadron distribution in a
 739 Fourier series with respect to the azimuthal angle ϕ [78],

$$E \frac{d^3 N}{d^3 p} = \frac{1}{2\pi} \frac{d^2 N}{p_t dp_t dy} \left(1 + \sum_{n=1}^{\infty} 2v_n \cos[n(\phi - \Psi_R)] \right), \quad (1.18)$$

740 where E is the energy of the particle, p is its momentum, p_T is the momentum
 741 component in the plane transverse to the beam axis, y is the particle's rapidity, and
 742 Ψ_R is the reaction plane angle. This reaction plane angle is defined by the beam axis
 743 and the impact parameter vector. The Fourier coefficients

$$v_n = \langle \cos[n(\phi - \Psi_R)] \rangle \quad (1.19)$$

744 determine the “strength” of the corresponding flow component. The first two co-
 745 efficients, v_1 and v_2 , are referred to as **directed (radial) flow** and **elliptic flow**,

746 respectively. A non-zero directed flow originates from the space-momentum correla-
 747 tions in particle production from a longitudinally slanted source [79]. Directed flow
 748 is often much smaller than elliptic flow (by over an order of magnitude) [80], but it
 749 can still effect some of the measurements presented in this thesis (see Section ?? for
 750 more details).

751 Elliptic flow characterizes the anisotropy of the particle production in the trans-
 752 verse plane. This anisotropy is believed to be caused by the initial anisotropy of the
 753 collision geometry, where the overlap region of the colliding nuclei forms an “almond”
 754 shape. This almond is where the initial QGP is formed, which then hydrodynamically
 755 expands and thermalizes nearly instantaneously. The initial spacial anisotropy results
 756 in unequal QGP path lengths for the constituent partons, which ultimately results in
 757 an anisotropic momentum distribution for the corresponding hadrons (i.e. partons
 758 which travel through more medium lose more energy, as discussed in Section 1.5.3).
 759 A diagram depicting this process can be seen in Figure 1.17.

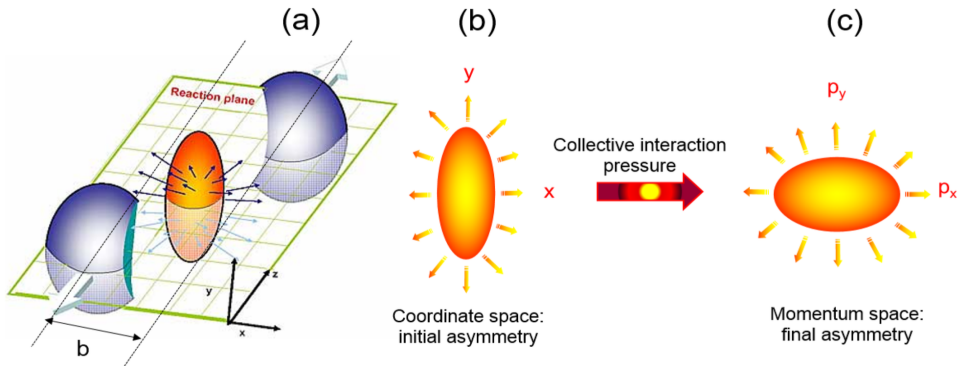


Figure 1.17: A schematic of the formation of elliptic flow in a heavy ion collision. The initial anisotropy in coordinate space results in a pressure gradient that causes a momentum space anisotropy in the final state hadrons.

760 1.5.4.1 Avoiding Ψ_R

761 Reconstructing the reaction plane angle Ψ_R is difficult as it must be done on an event-
 762 by-event basis [78]. As such, it is often more convenient to measure the collective
 763 flow components by looking at two-particle correlations in the azimuthal angle ϕ . In
 764 other words, the flow components can be obtained by looking at the distribution of

765 pairs of particles as a function of $\Delta\phi = \phi_1 - \phi_2$, where ϕ_1 and ϕ_2 are the azimuthal
766 angles of two (non-identical) particles. This distribution can be decomposed into a
767 Fourier series similar to Equation 1.18 [81],

$$\frac{dN^{\text{pair}}}{d\Delta\varphi} = a_0 + 2a_1 \cos \Delta\varphi + 2a_2 \cos 2\Delta\varphi + \dots, \quad (1.20)$$

768 where $v_n \equiv a_n/a_0$ are the very same flow coefficients from before. This bypasses the
769 need to reconstruct the reaction plane angle Ψ_R , but it also makes clear that any
770 analyses involving two-particle angular correlations (like the one presented in this
771 thesis) must be mindful of the presence of these coefficients (see Chapter ?? for more
772 details).

773 1.5.5 Strangeness enhancement

774 Experimentally, strangeness production is measured by looking at the abundance
775 of strange hadrons relative to non-strange hadrons, like pions. For central heavy
776 ion collisions—both at the LHC and RHIC—these strange/non-strange particle ratios
777 are found to be consistent with a hadron gas in both thermal *and* chemical equilib-
778 rium [82], [83]. As mentioned previously, this is a strong indication that the QGP
779 is formed in these collisions. Furthermore, these particle ratios as measured in lower
780 multiplicity pp collisions at the LHC are found to be consistent with statistical mod-
781 els *without* chemical equilibration [84], [85]. Under the strangeness enhancement
782 picture, this indicates that QGP formation does *not* occur in these lower multiplicity
783 pp collisions.

784 However, filling in the gaps between low multiplicity pp collisions and high multi-
785 plicity Pb–Pb collisions reveals a more complicated picture, as shown in Figure 1.18.
786 The particle ratios seem to be consistent with a smooth transition between the two
787 regimes, independent of collision system. In other words, the ratios in higher multi-
788 plicity pp and p–Pb collisions match up nicely with the ratios in lower multiplicity
789 Pb–Pb collisions. This indicates that the enhanced production of strange quarks is
790 not exclusive to heavy ion collisions; there is an “onset” of strangeness enhancement
791 occurring in lower multiplicity pp and p–Pb collisions. Furthermore, this enhancement
792 is seen to scale with the number of strange quarks in the hadron: the Ω baryon (sss)
793 exhibits the largest enhancement, while the proton (uud) sees virtually no increase.

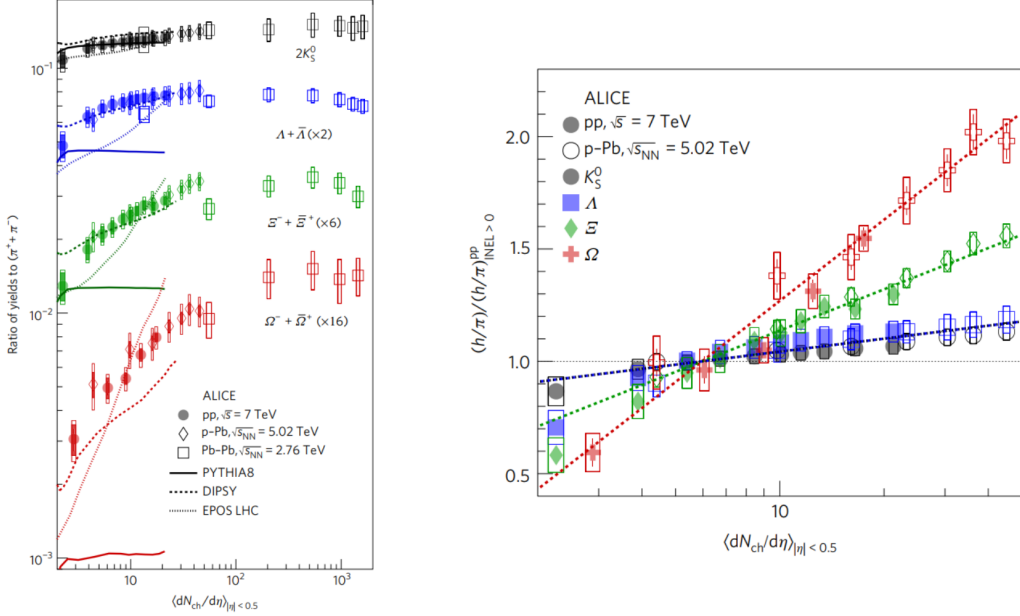


Figure 1.18: The particle ratios of strange hadrons to pions as a function multiplicity for different collision systems (left) and those same ratios normalized to an inclusive pp sample (right). The ratios appear to only depend on the multiplicity of the collision, and not the collision system. Taken from [86].

This provides even stronger evidence for the formation of a chemically equilibrated QGP, which no longer appears exclusive to heavy ion collisions.

While extensions to the aforementioned statistical models can describe these multiplicity-dependent particle ratios in a phenomenological manner [87], the microscopic origins of this enhancement are not well understood. By investigating the production of strange hadrons in p-Pb collisions (where the onset is greatest), this thesis aims to shed light on the origins of this strange enhancement. However, it is necessary to first introduce some theoretical models to help interpret the results of this thesis.

1.6 Heavy-Ion Collision Models

Theoretical models of heavy ion collisions are pertinent to the understanding of QCD and the QGP. Without them, there would be no framework for interpreting the results from the very expensive experiments dedicated to studying this strongly interacting

807 plasma. Unfortunately, due to the complexity of these heavy ion collision systems,
808 there is no *single* model that can describe the entire collision evolution. Instead,
809 the choice of model to compare a particular observable to depends very heavily on
810 the observable in question. For example, some models treat the QGP phase of the
811 collision as a hydrodynamic system, washing out information about the initial par-
812 tonic scatterings [88]. This can be useful when trying to study bulk properties of
813 the QGP (like the v_2 from Section ??), but not-so-useful when studying jets and
814 their constituents. Other models focus more on the individual partonic scatterings
815 and subsequent hadronization, but do not include an explicit QGP phase [89], [90].
816 Such models are powerful tools for analyzing smaller collision systems (pp and lower
817 multiplicity p–Pb), but fail to capture many of the features observed in heavy ion
818 collision data. In this section, the models used to help interpret the results of this
819 thesis will be discussed. All of these models are capable of simulating pp, p–Pb, and
820 Pb–Pb events.

821 1.6.1 PHSD

822 Parton-Hadron-String-Dynamics (PHSD) [91], [92] is the only model explored in this
823 thesis that utilizes a **microscopic transport approach**: it simulates the full space-
824 time evolution of a heavy-ion collision by modeling the interactions of individual
825 particles. Here “particles” refers to different quantities (strings, partons, hadrons)
826 which are all evolved in different ways. The transport equations of the partons and
827 hadrons are derived from the Kadanoff-Baym (KB) equations [93], which describe
828 the non-perturbative transport of particles in a strongly interacting system. The
829 evolution of a collision within PHSD is as follows.

830 1.6.1.1 Initial stages

831 Prior to the collision, the simulation is broken up into a 3D-grid of size 56 in each
832 of the x, y, and z directions. The total size of the grid increases with each time step
833 such that the number of particles within a given cell evolves smoothly with time. The
834 initial momentum distribution and abundances of partons within the nuclei (prior to
835 any collision) are given by the thermal distributions

$$f(\omega, \vec{p}) = C_i p^2 \omega \rho_i(\omega, \vec{p}) n_{F/B}(\omega/\tau), \quad (1.21)$$

836 where ρ_i are the spectral functions of the quarks and gluons ($i = q, \bar{q}, g$) and $n_{F/B}$ are
 837 the Fermi-Dirac (for quarks) and Bose-Einstein (for gluons) distributions. Once the
 838 nuclei collide, the partons interact with each other under the Lund string model to
 839 form *leading hadrons* (at large rapidity) and *pre-hadrons* (at midrapidity), as shown
 840 in Figure 1.19. The leading hadrons are immune to dissociation within the QGP,
 841 while the pre-hadrons are not.

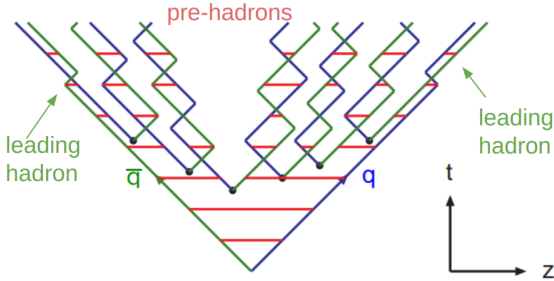


Figure 1.19: The Lund string model, with pre-hadrons and leading hadrons labeled.

842 1.6.1.2 QGP phase

843 If the energy density ϵ of a given cell increases beyond the critical energy density
 844 $\epsilon_c = 0.5 \text{ GeV/fm}^3$, the pre-hadrons within that cell are dissolved into partons. The
 845 partons are then treated as interacting quasi-particles under the DQPM [94] model,
 846 with Lorentzian spectral functions given by

$$\rho_j(\omega) = \frac{\gamma_j}{E_j} \left(\frac{1}{(\omega - E_j)^2 + \gamma_j^2} - \frac{1}{(\omega + E_j)^2 + \gamma_j^2} \right) \quad (1.22)$$

847 where i is one of (q, \bar{q}, g) and the width γ_i is given by

$$\gamma_g(T) = N_c \frac{g^2 T}{8\pi} \ln \frac{2c}{g^2}, \quad \gamma_q(T) = \frac{N_c^2 - 1}{2N_c} \frac{g^2 T}{8\pi} \ln \frac{2c}{g^2}, \quad (1.23)$$

848 where T is the temperature (calculated from the energy density within a given cell).
 849 This is the key difference between DQPM and other transport models—the quarks and
 850 gluons have non-zero temperature-dependent widths in the medium! The coupling
 851 constant g is also temperature dependent, and is of the form

$$g^2(T/T_c) = \frac{48\pi^2}{(11N_c - 2N_f) \ln (\lambda^2 (T/T_c - T_s/T_c)^2)}. \quad (1.24)$$

852 The parameters T_s and λ are fit to lattice QCD (lQCD) results [92]. The spectral
 853 functions are enough to describe the propagation of the mean-fields of the partons
 854 (effectively their Greens functions) via the aforementioned KB equations. The col-
 855 lisional terms in these equations are determined by the modified scattering cross
 856 sections of the partons. These cross sections are calculated using the leading order
 857 Feynman diagrams, with the DQPM-modified quark and gluon propagators given by

$$858 \quad i\delta_{ij} \frac{q + M_q}{q^2 - M_q^2 + 2i\gamma_q q_0} \quad (1.25)$$

858 and

$$-i\delta_{ab} \frac{g^{\mu\nu} - q^\mu q^\nu / M_g^2}{q^2 - M_g^2 + 2i\gamma_g q_0}, \quad (1.26)$$

859 respectively. Due to the large masses of the gluons, $q + \bar{q} \rightarrow g + g$ and $g \rightarrow g + g$ are
 860 suppressed and thus not included in the model.

861 1.6.1.3 Hadronization

862 Whenever the energy density of a given cell falls below the aforementioned critical
 863 energy density ($\epsilon_c = 0.5$ GeV/fm³), the partons within begin to hadronize. The
 864 dynamical hadronization of partons into hadrons is modeled by the equations

$$\begin{aligned} \frac{dN_m(x, p)}{d^4x d^4p} &= \text{Tr}_q \text{Tr}_{\bar{q}} \delta^4(p - p_q - p_{\bar{q}}) \delta^4\left(\frac{x_q + x_{\bar{q}}}{2} - x\right) \\ &\times \omega_q \rho_q(p_q) \omega_{\bar{q}} \rho_{\bar{q}}(p_{\bar{q}}) |v_{q\bar{q}}|^2 W_m(x_q - x_{\bar{q}}, (p_q - p_{\bar{q}})/2) \\ &\times N_q(x_q, p_q) N_{\bar{q}}(x_{\bar{q}}, p_{\bar{q}}) \delta(\text{ flavor, color }). \end{aligned} \quad (1.27)$$

865 for mesons and

$$\begin{aligned} \frac{dN_B(x, p)}{d^4x d^4p} &= \text{Tr}_{q_1} \text{Tr}_{q_2} \text{Tr}_{q_3} \delta^4(p - p_{\xi_3}) \delta^4(x - \xi_3) \delta\left(\sqrt{(\tau_1 - \tau_2)^2}\right) \\ &\times \omega_{q_1} \rho_{q_1}(p_1) \omega_{q_2} \rho_{q_2}(p_2) \omega_{q_3} \rho_{q_3}(p_3) \\ &\times |M_{qqq}|^2 W_B(\xi_1, \xi_2, p_{\xi_1}, p_{\xi_2}) \\ &\times N_{q_1}(x_1, p_1) N_{q_2}(x_2, p_2) N_{q_3}(x_3, p_3) \delta(\text{ flavor, color }). \end{aligned} \quad (1.28)$$

866 for baryons. The terms for the meson case are described as follows:

- 867 • Tr_q is shorthand notation for $\text{Tr}_q = \sum_q \int d^4x_q \int \frac{d^4p_q}{(2\pi)^4}$, where q is summed over
 868 all spin, color, and flavor degrees of freedom.

869 • $\delta^4(p - p_q - p_{\bar{q}})$ forces conservation of four-momentum. Note that the quarks
870 and anti-quarks are allowed to be off-shell (due to their non-zero widths), thus
871 this can result in off-shell mesons.

872 • $\delta^4\left(\frac{x_q+x_{\bar{q}}}{2} - x\right)$ puts the resulting meson in-between the quark and anti-quark
873 pair.

874 • ω_q and $\omega_{\bar{q}}$ are the energies of the quark and anti-quark, respectively.

875 • $\rho_q(p_q)$ and $\rho_{\bar{q}}(p_{\bar{q}})$ are the aforementioned spectral functions of the quark and
876 anti-quark, respectively.

877 • $|v_{q\bar{q}}|^2$ is the DQPM-determined *effective quark-anti-quark interaction*, which is
878 shown as the green dashed line in Figure 1.20. Note that this value is very small
879 for large quark (energy) densities, and thus this entire equation is effectively
880 zero. However, for low quark densities this value blows up, which “turns on” the
881 hadronization (and also guarantees that all partons will hadronize *eventually*).

882 • $W_m(x_q - x_{\bar{q}}, (p_q - p_{\bar{q}})/2)$ is the phase-space distribution of the resulting (pre-
883)meson

884 • $N_q(x_q, p_q)$ and $N_{\bar{q}}(x_{\bar{q}}, p_{\bar{q}})$ are the phase-space densities of the quark and anti-
885 quark, respectively.

886 • $\delta(\text{ flavor, color })$ is shorthand for “make sure flavor quantum numbers are con-
887 served and that the resulting meson is color-neutral”.

888 The terms for the baryon case are similar.

889 The numerical integrations of equations 1.27 and 1.28 for a fixed test parton
890 ultimately give the probability for a hadronization event to occur. From there, events
891 are randomly selected using Monte Carlo techniques, which give a color neutral state
892 with definite x, p and flavor. However, this is *still* not enough to specify a hadron
893 completely: many hadronic states of the same flavor have large widths. Thus to
894 determine the identity of the final hadron, the weight of each possible²⁴ hadronic

²⁴PHSD only includes the baryon octet/decouplet, the spin 0 and spin 1 meson nonets, and a few higher resonance states. Furthermore, if the invariant mass of the color neutral state is above 1.3 GeV (for mesons) or 1.5 GeV (for baryons), the state is treated as a Lund string with further decay handled by the JETSET algorithm [95]

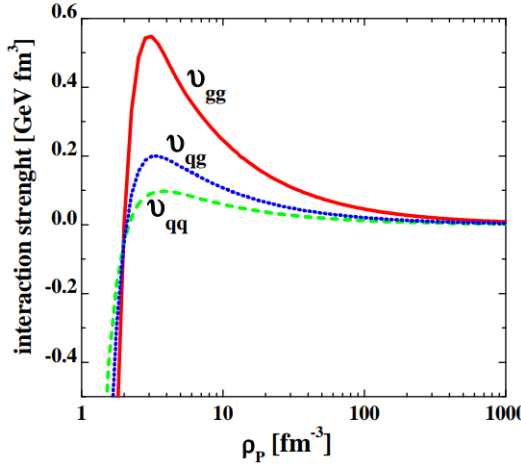


Figure 1.20: The effective quark-quark (green), quark-gluon (blue), and gluon-gluon (red) interactions as a function of parton density in DQPM, taken from [91].

895 spectral function is computed. The hadron is then randomly assigned an identity
 896 based on these weights using Monte Carlo.

897 1.6.1.4 Hadronic phase

898 All of the hadrons produced in the previous steps are transported using Hadron-
 899 String-Dynamics [96] (PHSD without the P). The phase-space distributions of the
 900 hadrons in HSD are transported using the equation

$$\begin{aligned} & \left\{ \left(\Pi_\mu - \Pi_\nu \partial_\mu^p U_h^\nu - M_h^* \partial_\mu^p U_h^S \right) \partial_x^\mu + \left(\Pi_\nu \partial_\mu^x U_h^\nu + M_h^* \partial_\mu^x U_h^S \right) \partial_p^\mu \right\} f_h(x, p) \\ &= \sum_{h_2 h_3 h_4 \dots} \int d2d3d4 \dots [G^\dagger G]_{12 \rightarrow 34 \dots} \delta_\Gamma^4 (\Pi + \Pi_2 - \Pi_3 - \Pi_4 \dots) \\ & \quad \times \left\{ f_{h_3}(x, p_3) f_{h_4}(x, p_4) \bar{f}_h(x, p) \bar{f}_{h_2}(x, p_2) \right. \\ & \quad \left. - f_h(x, p) f_{h_2}(x, p_2) \bar{f}_{h_3}(x, p_3) \bar{f}_{h_4}(x, p_4) \right\} \dots, \end{aligned} \tag{1.29}$$

901 where U_h^S and U_h^μ are the scalar and vector hadron self-energies, respectively. The
 902 effective mass of the hadron M_h^* is given by

$$M_h^* = M_h + U_h^S, \tag{1.30}$$

903 and its effective momentum is given by

$$\Pi^\mu = p^\mu - U_h^\mu. \tag{1.31}$$

904 The ‘‘collisional’’ term $[G^\dagger G]_{12 \rightarrow 34\dots}$ is the transition rate for the process $1 + 2 \rightarrow$
905 $3 + 4 + \dots$, which is modeled using Lund string fragmentation. The self-energies U_h^S
906 and U_h^μ are evaluated on the basis of a Nambu-Jona-Lasinio (NJL)-type model [97]
907 for the QCD Lagrangian. Once these self-energies (and $[G^\dagger G]_{12 \rightarrow 34\dots}$) are specified,
908 the transport equation (Equation 1.29) can be solved.

909 **1.6.1.5 A simple overview**

910 While the equations that govern PHSD are quite complicated, the overall picture is
911 relatively simple. It can be summarized as follows:

- 912 • First, the simulation is split up into cells whose sizes evolve with time, as shown
913 in Figure 1.21.
- 914 • As the initial nuclei collide, and the interacting partons form pre-hadrons and
915 leading hadrons.
- 916 • If the energy density of a cell is too high, the pre-hadrons dissolve into partons,
917 which are handled by the DQPM model.
- 918 • If a cell with partons in it cools off, the partons dynamically hadronize.
- 919 • The resulting hadrons (and any hadrons present in a particular cell) are trans-
920 ported using HSD.

921 **1.6.2 EPOS LHC**

922 In the EPOS LHC [98] model, the initial colliding nuclei results in many parton-
923 parton scatterings happening in parallel, as shown in Figure 1.22. These simultaneous
924 scatterings form a parton ladder, which are modeled as relativistic Lund strings. Long
925 before hadronization, the model separates into two distinct parts: the *core* and the
926 *corona*. This designation is based on the string density (i.e. the number of string
927 segments per unit volume). If the string density exceeds a critical density ρ_c , the
928 string segments are considered to be in the core. Otherwise, they are in the corona.

929 The core is evolved in a hydrodynamic manner, which loses all information about
930 the initial string segments and their interactions. Hadronization in the core is handled
931 by a microcanonical procedure known as Cooper-Frye freeze-out, which is described

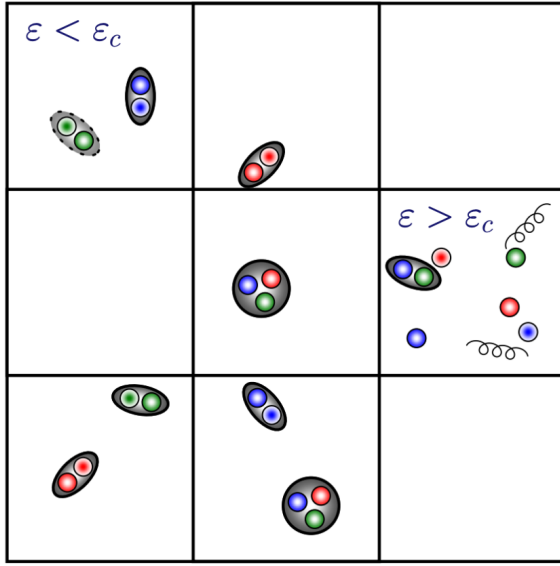


Figure 1.21: The cells within PHSD. If the energy density of the cell is greater than the critical energy density, the pre-hadrons dissolve into partons.

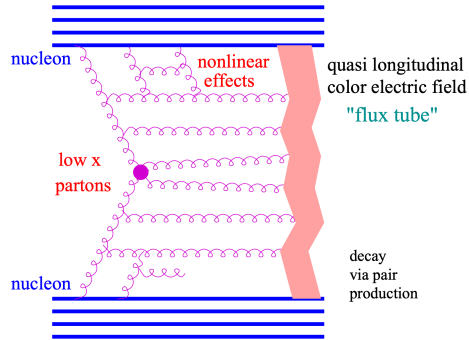


Figure 1.22: A schematic of the elementary interaction in EPOS LHC in which many parton-parton interactions are occurring simultaneously [98].

932 in detail in [99]. The core is associated with the QGP medium, and dominates particle
 933 production at higher multiplicities. The corona, however, corresponds to unmodified
 934 Lund string fragmentation, which dominates at large rapidity and in lower multiplicity
 935 events.

936 **1.6.3 DPMJET**

937 Perhaps the most simple²⁵ event generator explored in this thesis is the DPMJET [100]
938 model. DPMJET combines the Dual Parton Model (DPM) [101] with the Lund string
939 model [59] to describe proton-proton, proton-nucleus, and nucleus-nucleus collisions
940 across a large range of energies. The DPM describes all of the soft, non-perturbative
941 multi-particle events that occur within a heavy ion collision using various large N_c
942 and N_f limits of QCD. This is the only model explored in this thesis that does
943 not have an explicit QGP phase, as the collision constituents²⁶ are always treated
944 independently. Thus DPMJET serves as a good baseline for vacuum fragmentation,
945 and can be compared with other models (and data) to help quantify the effects of the
946 explicit QGP phase.

²⁵Still *extremely* complicated from a theoretical perspective, but has the least moving parts.

²⁶Strings. It's always strings.

Bibliography

- 948 [1] B. Pullman, *The Atom in the History of Human Thought*. Oxford: Oxford
949 University Press, 1998, ISBN: 978-0-19-515040-7 (cit. on p. 2).
- 950 [2] J. Dalton, “Experimental enquiry into the proportion of the several gases
951 or elastic fluids, constituting the atmosphere,” *Memoirs of the Literary and*
952 *Philosophical Society of Manchester*, vol. 1, pp. 244–258, 1805 (cit. on p. 2).
- 953 [3] E. R. Scerri, *The Periodic Table: A Very Short Introduction*. Oxford University
954 Press, Jul. 2019, pp. 117–123, ISBN: 9780198842323. DOI: 10.1093/actrade/
955 9780198842323.001.0001. [Online]. Available: <https://doi.org/10.1093/actrade/9780198842323.001.0001> (cit. on p. 2).
- 956 [4] D. Mendeleev, “The natural system of elements and its application to the
957 indication of the properties of undiscovered elements,” *Journal of the Russian
958 Chemical Society*, vol. 3, pp. 25–56, 1871 (cit. on p. 2).
- 959 [5] I. Falconer, “J J Thomson and the discovery of the electron,” *Physics Educa-
960 tion*, vol. 32, no. 4, p. 226, 1997. DOI: 10.1088/0031-9120/32/4/015.
961 [Online]. Available: <https://dx.doi.org/10.1088/0031-9120/32/4/015>
962 (cit. on p. 3).
- 963 [6] E. Rutherford, “The scattering of α and β particles by matter and the structure
964 of the atom,” *Philosophical Magazine Series 6*, vol. 21, pp. 669–688, 1911 (cit.
965 on p. 3).
- 966 [7] J. Chadwick, “Possible existence of a neutron,” *Nature*, vol. 129, p. 312, 1932
967 (cit. on p. 3).
- 968 [8] C. D. Anderson, “The apparent existence of easily deflectable positives,” *Sci-
969 ence*, vol. 76, no. 1967, pp. 238–239, 1932. DOI: 10.1126/science.76.1967.
970 238. eprint: <https://www.science.org/doi/pdf/10.1126/science.76.1967.238>. [Online]. Available: <https://www.science.org/doi/abs/10.1126/science.76.1967.238> (cit. on p. 3).
- 971
- 972
- 973

- 974 [9] S. H. Neddermeyer and C. D. Anderson, “Note on the nature of cosmic-ray
975 particles,” *Phys. Rev.*, vol. 51, pp. 884–886, 10 1937. DOI: 10.1103/PhysRev.
976 51.884. [Online]. Available: <https://link.aps.org/doi/10.1103/PhysRev.51.884> (cit. on p. 3).
- 978 [10] R. Brown *et al.*, “Observations with Electron-Sensitive Plates Exposed to
979 Cosmic Radiation,” *Nature*, vol. 163, no. 4133, pp. 82–87, Jan. 1949. DOI:
980 10.1038/163082a0 (cit. on p. 3).
- 981 [11] V. D. Hopper and S. Biswas, “Evidence concerning the existence of the new
982 unstable elementary neutral particle,” *Phys. Rev.*, vol. 80, pp. 1099–1100, 6
983 1950. DOI: 10.1103/PhysRev.80.1099. [Online]. Available: <https://link.aps.org/doi/10.1103/PhysRev.80.1099> (cit. on p. 3).
- 985 [12] A. Barbaro-Galtieri *et al.*, “Apparent violation of the $\Delta S = \Delta Q$ rule by lep-
986 tonic Σ^+ decay,” *Phys. Rev. Lett.*, vol. 9, pp. 26–29, 1 1962. DOI: 10.1103/
987 PhysRevLett.9.26. [Online]. Available: <https://link.aps.org/doi/10.1103/PhysRevLett.9.26> (cit. on p. 3).
- 989 [13] T. Nakano and K. Nishijima, “Charge Independence for V-particles,” *Progress
990 of Theoretical Physics*, vol. 10, no. 5, pp. 581–582, 1953. DOI: 10.1143/PTP.
991 10.581 (cit. on p. 3).
- 992 [14] R. Serway, C. Moses, and C. Moyer, *Modern Physics*. Cengage Learning, 2004,
993 pp. 12–13, ISBN: 9780534493394. [Online]. Available: <https://books.google.com/books?id=Yfo3rnt3bkEC> (cit. on p. 3).
- 995 [15] M. Gell-Mann, “The Eightfold Way: A theory of strong interaction symmetry,”
996 Mar. 1961. DOI: 10.2172/4008239. [Online]. Available: <https://www.osti.gov/biblio/4008239> (cit. on pp. 3, 4, 11).
- 998 [16] Y. Ne’eman, “Derivation of strong interactions from a gauge invariance,” *Nu-
999 clear Physics*, vol. 26, no. 2, pp. 222–229, 1961. DOI: 10.1016/0029-5582(61)
1000 90134-1 (cit. on p. 3).
- 1001 [17] W. Heisenberg, “Über den Bau der Atomkerne. I,” *Zeitschrift fur Physik*,
1002 vol. 77, no. 1-2, pp. 1–11, Jan. 1932. DOI: 10.1007/BF01342433 (cit. on
1003 p. 3).

- 1004 [18] M. Gell-Mann, “Isotopic Spin and New Unstable Particles,” *Physical Review*,
1005 vol. 92, no. 3, pp. 833–834, Nov. 1953. DOI: 10.1103/PhysRev.92.833 (cit. on
1006 pp. 3, 23, 24, 31).
- 1007 [19] T. Nakano and K. Nishijima, “Charge Independence for V-particles,” *Progress*
1008 *of Theoretical Physics*, vol. 10, no. 5, pp. 581–582, Nov. 1953. DOI: 10.1143/
1009 PTP.10.581 (cit. on p. 4).
- 1010 [20] M. Gell-Mann, “The interpretation of the new particles as displaced charge
1011 multiplets,” *Il Nuovo Cimento*, vol. 4, no. S2, pp. 848–866, Apr. 1956. DOI:
1012 10.1007/BF02748000 (cit. on p. 4).
- 1013 [21] M. Gell-Mann, “A schematic model of baryons and mesons,” *Physics Letters*,
1014 vol. 8, no. 3, pp. 214–215, Feb. 1964. DOI: 10.1016/S0031-9163(64)92001-3
1015 (cit. on p. 4).
- 1016 [22] A. Pickering, *Constructing quarks*. University of Chicago Press, 1999, pp. 114–
1017 125. DOI: 10.7208/chicago/9780226667997.003.0007 (cit. on p. 5).
- 1018 [23] B. J. Bjørken and S. L. Glashow, “Elementary particles and SU(4),” *Physics*
1019 *Letters*, vol. 11, no. 3, pp. 255–257, Aug. 1964. DOI: 10.1016/0031-9163(64)
1020 90433-0 (cit. on p. 5).
- 1021 [24] S. Glashow, “The hunting of the atoms and their nuclei: Protons and neu-
1022 trons,” *New York Times*, Jul. 1976. [Online]. Available: <https://www.nytimes.com/1976/07/18/archives/the-hunting-of-the-atoms-and-their-nuclei-protons-and-neutrons.html> (cit. on p. 5).
- 1025 [25] S. L. Glashow, J. Iliopoulos, and L. Maiani, “Weak Interactions with Lepton-
1026 Hadron Symmetry,” *Phys Rev D*, vol. 2, no. 7, pp. 1285–1292, Oct. 1970. DOI:
1027 10.1103/PhysRevD.2.1285 (cit. on p. 5).
- 1028 [26] H. Kendall, *Deep inelastic scattering: Experiments on the proton and the ob-
1029 servation of scaling*, 1990. [Online]. Available: <https://www.nobelprize.org/uploads/2018/06/kendall-lecture.pdf> (visited on 08/21/2023) (cit.
1030 on pp. 5, 6).
- 1032 [27] J. Friedman, *Deep inelastic scattering: Comparisons with the quark model*,
1033 1990. [Online]. Available: <https://www.nobelprize.org/uploads/2018/06/friedman-lecture.pdf> (visited on 08/21/2023) (cit. on p. 5).

- 1035 [28] R. Taylor, *Deep inelastic scattering: The early years*, 1990. [Online]. Available:
1036 <https://www.nobelprize.org/uploads/2018/06/taylor-lecture.pdf>
1037 (visited on 08/21/2023) (cit. on p. 5).
- 1038 [29] E. D. Bloom *et al.*, “High-Energy Inelastic e-p Scattering at 6° and 10° ,”
1039 *Physical Review Letters*, vol. 23, no. 16, pp. 930–934, Oct. 1969. DOI: 10.
1040 1103/PhysRevLett.23.930 (cit. on p. 5).
- 1041 [30] E. D. Bloom *et al.*, “High-Energy Inelastic e-p Scattering at 6° and 10° ,”
1042 *Physical Review Letters*, vol. 23, no. 16, pp. 930–934, Oct. 1969. DOI: 10.
1043 1103/PhysRevLett.23.930 (cit. on p. 5).
- 1044 [31] J. Bjorken, “Current algebra at small distances,” Jun. 2018. [Online]. Available:
1045 <https://www.osti.gov/biblio/1444446> (cit. on p. 6).
- 1046 [32] R. P. Feynman, “The behavior of hadron collisions at the uncertainties from
1047 these sources exhibit no multiplicity dependence, and a very small depen-
1048 dence on p_T . extreme energies,” in *Special Relativity and Quantum Theory:*
1049 *A Collection of Papers on the Poincaré Group*, M. E. Noz and Y. S. Kim,
1050 Eds. Dordrecht: Springer Netherlands, 1988, pp. 289–304, ISBN: 978-94-009-
1051 3051-3. DOI: 10.1007/978-94-009-3051-3_25. [Online]. Available: https://doi.org/10.1007/978-94-009-3051-3_25 (cit. on p. 6).
- 1053 [33] J. Aubert *et al.*, “Experimental observation of a heavy particle J ,” *Physical*
1054 *Review Letters*, vol. 33, Dec. 1974 (cit. on p. 6).
- 1055 [34] H. Fritzsch, M. Gell-Mann, and H. Leutwyler, “Advantages of the color octet
1056 gluon picture,” *Physics Letters B*, vol. 47, no. 4, pp. 365–368, Nov. 1973. DOI:
1057 10.1016/0370-2693(73)90625-4 (cit. on p. 7).
- 1058 [35] D. J. Gross and F. Wilczek, “Ultraviolet Behavior of Non-Abelian Gauge The-
1059 ories,” *Physical Review Letters*, vol. 30, no. 26, pp. 1343–1346, Jun. 1973. DOI:
1060 10.1103/PhysRevLett.30.1343 (cit. on p. 7).
- 1061 [36] H. D. Politzer, “Reliable Perturbative Results for Strong Interactions?” *Phys-*
1062 *ical Review Letters*, vol. 30, no. 26, pp. 1346–1349, Jun. 1973. DOI: 10.1103/
1063 PhysRevLett.30.1346 (cit. on p. 7).
- 1064 [37] P. Söding, *Twenty-five years of gluons*, 2004. [Online]. Available: <https://cerncourier.com/a/twenty-five-years-of-gluons/> (cit. on pp. 7, 14).

- 1066 [38] P. Söding, “On the discovery of the gluon,” *European Physical Journal H*,
1067 vol. 35, no. 1, pp. 3–28, Jul. 2010. DOI: 10.1140/epjh/e2010-00002-5 (cit.
1068 on p. 7).
- 1069 [39] A. Salam and J. C. Ward, “Weak and electromagnetic interactions,” *Il Nuovo
1070 Cimento*, vol. 11, no. 4, pp. 568–577, Feb. 1959. DOI: 10.1007/BF02726525
1071 (cit. on p. 7).
- 1072 [40] S. Weinberg, “A Model of Leptons,” *Physical Review Letters*, vol. 19, no. 21,
1073 pp. 1264–1266, Nov. 1967. DOI: 10.1103/PhysRevLett.19.1264 (cit. on p. 7).
- 1074 [41] P. W. Higgs, “Broken symmetries and the masses of gauge bosons,” *Phys. Rev.
1075 Lett.*, vol. 13, pp. 508–509, 16 1964. DOI: 10.1103/PhysRevLett.13.508.
1076 [Online]. Available: [https://link.aps.org/doi/10.1103/PhysRevLett.
1077 13.508](https://link.aps.org/doi/10.1103/PhysRevLett.13.508) (cit. on pp. 7–9).
- 1078 [42] P. T. Smith, “Reporting New Evidence of Gravitons,” in *14th International
1079 Symposium on Nuclei in the Cosmos (NIC2016)*, S. Kubono *et al.*, Eds., Jan.
1080 2017, 020101, p. 020101. DOI: 10.7566/JPSCP.14.020101 (cit. on p. 7).
- 1081 [43] G. Jungman, M. Kamionkowski, and K. Griest, “Supersymmetric dark matter,”
1082 *Physics Reports*, vol. 267, no. 5, pp. 195–373, 1996, ISSN: 0370-1573.
1083 DOI: [https://doi.org/10.1016/0370-1573\(95\)00058-5](https://doi.org/10.1016/0370-1573(95)00058-5). [Online].
1084 Available: [https://www.sciencedirect.com/science/article/pii/
1085 0370157395000585](https://www.sciencedirect.com/science/article/pii/0370157395000585) (cit. on p. 7).
- 1086 [44] G. Esposito, *An introduction to quantum gravity*, 2011. arXiv: 1108.3269
1087 [hep-th] (cit. on p. 8).
- 1088 [45] G. Aad *et al.*, “Observation of a new particle in the search for the Standard
1089 Model Higgs boson with the ATLAS detector at the LHC,” *Phys. Lett. B*,
1090 vol. 716, pp. 1–29, 2012. DOI: 10.1016/j.physletb.2012.08.020. arXiv:
1091 1207.7214 [hep-ex] (cit. on p. 9).
- 1092 [46] S. Chatrchyan *et al.*, “Observation of a New Boson at a Mass of 125 GeV
1093 with the CMS Experiment at the LHC,” *Phys. Lett. B*, vol. 716, pp. 30–61,
1094 2012. DOI: 10.1016/j.physletb.2012.08.021. arXiv: 1207.7235 [hep-ex]
1095 (cit. on p. 9).

- 1096 [47] R. Shivni, *The deconstructed standard model equation*, Sep. 2023. [Online].
1097 Available: https://www.symmetrymagazine.org/article/the-deconstructed-standard-model-equation?language_content_entity=und (cit. on p. 10).
- 1099 [48] F. Gross *et al.*, “50 Years of Quantum Chromodynamics,” Dec. 2022. arXiv:
1100 2212.11107 [hep-ph] (cit. on pp. 10, 11).
- 1101 [49] Wikipedia, *Structure constants — Wikipedia, the free encyclopedia*, <http://en.wikipedia.org/w/index.php?title=Structure%20constants&oldid=1160301276>, [Online; accessed 07-October-2023], 2023 (cit. on p. 11).
- 1104 [50] K. Chetyrkin and A. Rétey, “Renormalization and running of quark mass
1105 and field in the regularization invariant and schemes at three and four loops,”
1106 *Nuclear Physics B*, vol. 583, no. 1-2, pp. 3–34, Sep. 2000. DOI: 10.1016/s0550-
1107 3213(00)00331-x. [Online]. Available: <https://doi.org/10.1016%2Fs0550-3213%2800%2900331-x> (cit. on p. 12).
- 1109 [51] S. Weinberg, “New Approach to the Renormalization Group,” *Phys. Rev. D*,
1110 vol. 8, no. 10, pp. 3497–3509, Nov. 1973. DOI: 10.1103/PhysRevD.8.3497
1111 (cit. on p. 12).
- 1112 [52] R. L. Workman *et al.*, “Review of Particle Physics,” *PTEP*, vol. 2022, p. 083C01,
1113 2022. DOI: 10.1093/ptep/ptac097 (cit. on pp. 12, 14, 16, 20).
- 1114 [53] C. G. Callan, R. F. Dashen, and D. J. Gross, “The structure of the gauge
1115 theory vacuum,” *Physics Letters B*, vol. 63, no. 3, pp. 334–340, Aug. 1976.
1116 DOI: 10.1016/0370-2693(76)90277-X (cit. on p. 12).
- 1117 [54] J. L. Rosner, “CP symmetry violation,” Sep. 2001. arXiv: hep-ph/0109240
1118 (cit. on p. 12).
- 1119 [55] R. D. Peccei, “The Strong CP problem and axions,” *Lect. Notes Phys.*, vol. 741,
1120 M. Kuster, G. Raffelt, and B. Beltran, Eds., pp. 3–17, 2008. DOI: 10.1007/
1121 978-3-540-73518-2_1. arXiv: hep-ph/0607268 (cit. on p. 12).
- 1122 [56] J. J. Lodder, “On gluon masses, color symmetry, and a possible massive ninth
1123 gluon,” Jun. 1996. arXiv: hep-ph/9606317 (cit. on p. 12).
- 1124 [57] ”. Griffiths”, *Introduction to Elementary Particles*, ”2nd”. ”Wiley-VCH”,
1125 ”2008”, pp. 280–281, ISBN: ”978-3-527-40601-2” (cit. on p. 12).

- 1126 [58] T. Luthe, A. Maier, P. Marquard, and Y. Schroder, “Complete renormaliza-
 1127 tion of QCD at five loops,” *JHEP*, vol. 03, p. 020, 2017. DOI: 10.1007/
 1128 JHEP03(2017)020. arXiv: 1701.07068 [hep-ph] (cit. on p. 13).
- 1129 [59] B. Andersson, G. Gustafson, G. Ingelman, and T. Sjöstrand, “Parton frag-
 1130 mentation and string dynamics,” *Phys. Rep.*, vol. 97, no. 2-3, pp. 31–145,
 1131 Jul. 1983. DOI: 10.1016/0370-1573(83)90080-7 (cit. on pp. 13, 44).
- 1132 [60] ”. Wilson and others”, “superconducting accelerator research and develop-
 1133 ment at slac”, ”SLAC-PUB”, vol. ”749”, ”1970” (cit. on p. 14).
- 1134 [61] J. R. Finger and J. E. Mandula, “Quark pair condensation and chiral symme-
 1135 try breaking in QCD,” *Nuclear Physics B*, vol. 199, no. 1, pp. 168–188, 1982,
 1136 ISSN: 0550-3213. DOI: [https://doi.org/10.1016/0550-3213\(82\)90570-3](https://doi.org/10.1016/0550-3213(82)90570-3).
 1137 [Online]. Available: <https://www.sciencedirect.com/science/article/pii/0550321382905703> (cit. on p. 15).
- 1139 [62] R. K. Ellis, W. J. Stirling, and B. R. Webber, *QCD and Collider Physics*
 1140 (Cambridge Monographs on Particle Physics, Nuclear Physics and Cosmol-
 1141 ogy). Cambridge University Press, 1996. DOI: 10.1017/CBO9780511628788
 1142 (cit. on p. 17).
- 1143 [63] U. W. Heinz, “The Strongly coupled quark-gluon plasma created at RHIC,”
 1144 *J. Phys. A*, vol. 42, D. Neilson and G. Senatore, Eds., p. 214003, 2009. DOI:
 1145 10.1088/1751-8113/42/21/214003. arXiv: 0810.5529 [nucl-th] (cit. on
 1146 p. 18).
- 1147 [64] J. Letessier and J. Rafelski, *Hadrons and Quark-Gluon Plasma*. Oxford Uni-
 1148 versity Press, 2002, ISBN: 978-1-00-929075-3, 978-0-511-53499-7, 978-1-00-929070-
 1149 8, 978-1-00-929073-9. DOI: 10.1017/9781009290753 (cit. on p. 18).
- 1150 [65] A. Maire, “Phase diagram of QCD matter : Quark-Gluon Plasma,” General
 1151 Photo, 2015. [Online]. Available: <https://cds.cern.ch/record/2025215>
 1152 (cit. on p. 18).
- 1153 [66] J. Rafelski, “Connecting QGP-Heavy Ion Physics to the Early Universe,”
 1154 *Nucl. Phys. B Proc. Suppl.*, vol. 243-244, R. Battiston and S. Bertolucci, Eds.,
 1155 pp. 155–162, 2013. DOI: 10.1016/j.nuclphysbps.2013.09.017. arXiv:
 1156 1306.2471 [astro-ph.CO] (cit. on p. 19).

- 1157 [67] E. Annala *et al.*, “Evidence for quark-matter cores in massive neutron stars,”
1158 *Nature Phys.*, vol. 16, no. 9, pp. 907–910, 2020. DOI: 10.1038/s41567-020-
1159 0914-9. arXiv: 1903.09121 [astro-ph.HE] (cit. on p. 19).
- 1160 [68] F.-M. Liu and S.-X. Liu, “Quark-gluon plasma formation time and direct
1161 photons from heavy ion collisions,” *Phys. Rev. C*, vol. 89, no. 3, p. 034906,
1162 2014. DOI: 10.1103/PhysRevC.89.034906. arXiv: 1212.6587 [nucl-th]
1163 (cit. on pp. 25, 26).
- 1164 [69] Aug. 2021. [Online]. Available: <https://cerncourier.com/a/participants-and-spectators-at-the-heavy-ion-fireball/> (cit. on p. 28).
- 1166 [70] B. Abelev *et al.*, “Centrality determination of Pb-Pb collisions at $\sqrt{s_{NN}} =$
1167 2.76 TeV with ALICE,” *Phys. Rev. C*, vol. 88, no. 4, p. 044909, 2013. DOI:
1168 10.1103/PhysRevC.88.044909. arXiv: 1301.4361 [nucl-ex] (cit. on p. 29).
- 1169 [71] “Centrality determination in heavy ion collisions,” Aug. 2018 (cit. on pp. 29,
1170 30).
- 1171 [72] M. L. Miller, K. Reygers, S. J. Sanders, and P. Steinberg, “Glauber modeling
1172 in high energy nuclear collisions,” *Ann. Rev. Nucl. Part. Sci.*, vol. 57, pp. 205–
1173 243, 2007. DOI: 10.1146/annurev.nucl.57.090506.123020. arXiv: nucl-
1174 ex/0701025 (cit. on p. 29).
- 1175 [73] D. J. Gross and F. Wilczek, “Ultraviolet Behavior of Non-Abelian Gauge The-
1176 ories,” *Phys. Rev. Lett.*, vol. 30, no. 26, pp. 1343–1346, Jun. 1973. DOI:
1177 10.1103/PhysRevLett.30.1343 (cit. on p. 30).
- 1178 [74] H. Stoecker, “Collective flow signals the quark gluon plasma,” *Nucl. Phys. A*,
1179 vol. 750, D. Rischke and G. Levin, Eds., pp. 121–147, 2005. DOI: 10.1016/j.
1180 nuclphysa.2004.12.074. arXiv: nucl-th/0406018 (cit. on p. 30).
- 1181 [75] S. Cao and X.-N. Wang, “Jet quenching and medium response in high-energy
1182 heavy-ion collisions: a review,” *Rept. Prog. Phys.*, vol. 84, no. 2, p. 024301,
1183 2021. DOI: 10.1088/1361-6633/abc22b. arXiv: 2002.04028 [hep-ph] (cit.
1184 on p. 31).
- 1185 [76] A. Collaboration, “ATLAS Feature: Looking inside trillion degree matter,”
1186 General Photo, 2022. [Online]. Available: <https://cds.cern.ch/record/2809432> (cit. on p. 32).

- 1188 [77] C. Adler *et al.*, “Disappearance of back-to-back high p_T hadron correlations
 1189 in central Au+Au collisions at $\sqrt{s_{NN}} = 200\text{-GeV}$,” *Phys. Rev. Lett.*, vol. 90,
 1190 p. 082302, 2003. DOI: 10.1103/PhysRevLett.90.082302. arXiv: nucl-ex/0210033 (cit. on pp. 32, 33).
- 1192 [78] K. Aamodt *et al.*, “Elliptic flow of charged particles in Pb-Pb collisions at 2.76
 1193 TeV,” *Phys. Rev. Lett.*, vol. 105, p. 252302, 2010. DOI: 10.1103/PhysRevLett.
 1194 105.252302. arXiv: 1011.3914 [nucl-ex] (cit. on pp. 33, 34).
- 1195 [79] P. Bo ţek, “Splitting of proton-antiproton directed flow in relativistic heavy-
 1196 ion collisions,” *Phys. Rev. C*, vol. 106, p. L061901, 6 Dec. 2022. DOI: 10.1103/
 1197 PhysRevC.106.L061901. [Online]. Available: <https://link.aps.org/doi/10.1103/PhysRevC.106.L061901> (cit. on p. 34).
- 1199 [80] M. Luzum and J.-Y. Ollitrault, “Directed flow at midrapidity in heavy-ion col-
 1200 lisions,” *Phys. Rev. Lett.*, vol. 106, p. 102301, 2011. DOI: 10.1103/PhysRevLett.
 1201 106.102301. arXiv: 1011.6361 [nucl-ex] (cit. on p. 34).
- 1202 [81] A. M. Poskanzer and S. A. Voloshin, “Methods for analyzing anisotropic flow
 1203 in relativistic nuclear collisions,” *Phys. Rev. C*, vol. 58, pp. 1671–1678, 3 Sep.
 1204 1998. DOI: 10.1103/PhysRevC.58.1671. [Online]. Available: <https://link.aps.org/doi/10.1103/PhysRevC.58.1671> (cit. on p. 35).
- 1206 [82] J. Cleymans *et al.*, “Statistical model predictions for particle ratios at $s(\text{NN})^{**}(1/2)$
 1207 $= 5.5\text{-TeV}$,” *Phys. Rev. C*, vol. 74, p. 034903, 2006. DOI: 10.1103/PhysRevC.
 1208 74.034903. arXiv: hep-ph/0604237 (cit. on p. 35).
- 1209 [83] A. Andronic, P. Braun-Munzinger, and J. Stachel, “Thermal hadron produc-
 1210 tion in relativistic nuclear collisions,” *Acta Phys. Polon. B*, vol. 40, pp. 1005–
 1211 1012, 2009. arXiv: 0901.2909 [nucl-th] (cit. on p. 35).
- 1212 [84] R. Hagedorn and J. Ranft, “Statistical thermodynamics of strong interactions
 1213 at high-energies. 2. Momentum spectra of particles produced in pp-collisions,”
 1214 *Nuovo Cim. Suppl.*, vol. 6, pp. 169–354, 1968 (cit. on p. 35).
- 1215 [85] F. Becattini and U. W. Heinz, “Thermal hadron production in p p and p anti-
 1216 p collisions,” *Z. Phys. C*, vol. 76, pp. 269–286, 1997, [Erratum: Z.Phys.C 76,
 1217 578 (1997)]. DOI: 10.1007/s002880050551. arXiv: hep-ph/9702274 (cit. on
 1218 p. 35).

- 1219 [86] J. Adam *et al.*, “Enhanced production of multi-strange hadrons in high-multiplicity
 1220 proton-proton collisions,” *Nature Phys.*, vol. 13, pp. 535–539, 2017. DOI: 10.
 1221 1038/nphys4111. arXiv: 1606.07424 [nucl-ex] (cit. on p. 36).
- 1222 [87] F. Becattini and J. Manninen, “Strangeness production from SPS to LHC,” *J.
 1223 Phys. G*, vol. 35, J.-e. Alam *et al.*, Eds., p. 104013, 2008. DOI: 10.1088/0954-
 1224 3899/35/10/104013. arXiv: 0805.0098 [nucl-th] (cit. on p. 36).
- 1225 [88] T. Pierog and K. Werner, “EPOS Model and Ultra High Energy Cosmic Rays,”
 1226 *Nucl. Phys. B Proc. Suppl.*, vol. 196, J.-N. Capdevielle, R. Engel, and B.
 1227 Pattison, Eds., pp. 102–105, 2009. DOI: 10.1016/j.nuclphysbps.2009.09.
 1228 017. arXiv: 0905.1198 [hep-ph] (cit. on p. 37).
- 1229 [89] C. Bierlich *et al.*, “A comprehensive guide to the physics and usage of PYTHIA
 1230 8.3,” Mar. 2022. DOI: 10.21468/SciPostPhysCodeb.8. arXiv: 2203.11601
 1231 [hep-ph] (cit. on p. 37).
- 1232 [90] S. Roesler, R. Engel, and J. Ranft, “The Monte Carlo event generator DPMJET-
 1233 III,” in *International Conference on Advanced Monte Carlo for Radiation
 1234 Physics, Particle Transport Simulation and Applications (MC 2000)*, Dec.
 1235 2000, pp. 1033–1038. DOI: 10.1007/978-3-642-18211-2_166. arXiv: hep-
 1236 ph/0012252 (cit. on p. 37).
- 1237 [91] W. Cassing and E. L. Bratkovskaya, “Parton transport and hadronization from
 1238 the dynamical quasiparticle point of view,” *Phys. Rev. C*, vol. 78, p. 034919,
 1239 2008. DOI: 10.1103/PhysRevC.78.034919. arXiv: 0808.0022 [hep-ph] (cit.
 1240 on pp. 37, 41).
- 1241 [92] W. Cassing and E. L. Bratkovskaya, “Parton-Hadron-String Dynamics: an
 1242 off-shell transport approach for relativistic energies,” *Nucl. Phys. A*, vol. 831,
 1243 pp. 215–242, 2009. DOI: 10.1016/j.nuclphysa.2009.09.007. arXiv: 0907.
 1244 5331 [nucl-th] (cit. on pp. 37, 39).
- 1245 [93] W. Cassing, “From Kadanoff-Baym dynamics to off-shell parton transport,”
 1246 *Eur. Phys. J. ST*, vol. 168, R. Alkofer, H. Gies, and B.-J. Schaefer, Eds., pp. 3–
 1247 87, 2009. DOI: 10.1140/epjst/e2009-00959-x. arXiv: 0808.0715 [nucl-th]
 1248 (cit. on p. 37).

- 1249 [94] O. Soloveva, J. Aichelin, and E. Bratkovskaya, “Transport properties and
1250 equation-of-state of hot and dense QGP matter near the critical endpoint in
1251 the phenomenological dynamical quasiparticle model,” *Phys. Rev. D*, vol. 105,
1252 no. 5, p. 054011, 2022. DOI: 10.1103/PhysRevD.105.054011. arXiv: 2108.
1253 08561 [hep-ph] (cit. on p. 38).
- 1254 [95] T. Sjostrand, “PYTHIA 5.7 and JETSET 7.4: Physics and manual,” Feb. 1994.
1255 arXiv: hep-ph/9508391 (cit. on p. 40).
- 1256 [96] W. Ehehalt and W. Cassing, “Relativistic transport approach for nucleus nu-
1257 cleus collisions from SIS to SPS energies,” *Nucl. Phys. A*, vol. 602, pp. 449–
1258 486, 1996. DOI: 10.1016/0375-9474(96)00097-8 (cit. on p. 41).
- 1259 [97] Y. Nambu and G. Jona-Lasinio, “Dynamical Model of Elementary Particles
1260 Based on an Analogy with Superconductivity. I,” *Physical Review*, vol. 122,
1261 no. 1, pp. 345–358, Apr. 1961. DOI: 10.1103/PhysRev.122.345 (cit. on p. 42).
- 1262 [98] T. Pierog *et al.*, “Epos lhc: Test of collective hadronization with data measured
1263 at the cern large hadron collider,” *Phys. Rev. C*, vol. 92, p. 034906, 3 Sep.
1264 2015. DOI: 10.1103/PhysRevC.92.034906. [Online]. Available: <https://link.aps.org/doi/10.1103/PhysRevC.92.034906> (cit. on pp. 42, 43).
- 1266 [99] Z. Wolff and D. Molnar, “Self-consistent Cooper-Frye freeze-out of a viscous
1267 fluid to particles,” *J. Phys. Conf. Ser.*, vol. 535, p. 012020, 2014. DOI: 10.
1268 1088/1742-6596/535/1/012020. arXiv: 1407.6413 [nucl-th] (cit. on p. 43).
- 1269 [100] S. Roesler, R. Engel, and J. Ranft, “The monte carlo event generator DPMJET-
1270 III,” in *Advanced Monte Carlo for Radiation Physics, Particle Transport Sim-
1271 ulation and Applications*, Springer Berlin Heidelberg, 2001. arXiv: 0012252
1272 [hep-ph] (cit. on p. 44).
- 1273 [101] A. Capella, U. Sukhatme, C.-I. Tan, and J. Tran Thanh Van, “Dual par-
1274 ton model,” *Phys. Rept.*, vol. 236, pp. 225–329, 1994. DOI: 10.1016/0370-
1275 1573(94)90064-7 (cit. on p. 44).